Bayesian data-driven framework for structural health monitoring of composite structures under limited experimental data

Leonardo de Paula Silva Ferreira, Rafaël Teloli, Samuel da Silva, Eloi Figueiredo, Nuno Maia, Carlos Alberto Cimini Jr

Journal Title
XX(X):1–21

DOI: 10.1177/ToBeAssigned
www.sagepub.com/
SAGE

Bayesian data-driven framework for structural health monitoring of composite structures under limited experimental data

Leonardo Ferreira[1], Rafael de O. Teloli[2], Samuel da Silva[3], Eloi Figueiredo [4,5], Nuno Maia [6] and Carlos Cimini [1]

Abstract

Ultrasonic-guided waves help monitor the health of thin-walled structures. However, damage tests on materials like carbon fiber-reinforced plastics are impractical and costly. Instead, numerical modeling is suggested to create hybrid datasets for machine learning training, integrating data from numerical and experimental tests. This paper presents a Bayesian-driven framework to compensate for limited experimental data regarding Lamb wave propagation in composite plates. Using Bayesian inference, the framework refines a numerical FE model, considering observed uncertainties and employing Markov-Chain Monte Carlo simulations and the Metropolis-Hastings algorithm. A neural network fast-tracks these simulations, leading to a model that reflects the uncertain experimental setup. This model then generates data to augment true experimental data. Finally, a 1D deep convolutional neural network is trained on a hybrid dataset to analyze Lamb wave signals and assess damage. Comparing training strategies shows the hybrid approach proposes the most accurate damage size predictions.

Keywords

Structural health monitoring, composite materials, Bayesian calibration, machine learning, convolutional neural networks

Introduction

Structural health monitoring (SHM) has evolved from heuristic condition assessments, offering real-time monitoring systems that detect early anomalies or damage in aerospace, civil, or mechanical structures. As described by Farrar et al.[1], damage entails changes compromising the structure's performance and safety. Two core SHM methods exist: (i) the physics-based approach, using inverse problem techniques and finite element (FE) models to understand physical relations, and (ii) the data-based approach, which relies on machine learning algorithms to interpret structural behavior from past data, mainly when physics-based solutions are impractical due to accuracy or efficiency limits. Available algorithm options include K-nearest neighbor[2], support vector machines (SVM)[3], and artificial neural networks (ANNs)[4,5]. Among these, neural networks implemented in various architectures like Multi-Layer Perceptron (MLP), Long Short Term Memory (LSTM), and Convolutional Neural Network (CNN) have found applications in domains like image classification and natural language processing. In the domain of SHM, a particular focus has been placed on assessing plate-like structures using Lamb waves.

Lamb waves are a form of ultrasonic-guided elastic waves that travel through thin plates and laminates. They have been key for SHM in evaluating the operational conditions of plate-like structures. Due to their ability to propagate over long distances, they are suitable for local inspections, such as detecting fatigue[6], corrosion[7], and assembled joints[8], as well as for assessing large-scale structures in the aerospace industry[9]. This work focuses on Lamb wave propagation in composite structures[10]. However, analyzing composite materials presents inherent challenges owing to their natural heterogeneity and the myriad layout possibilities affecting wave propagation patterns. Further complexities arise as the physical properties of composites, such as elasticity and shear moduli, shift with environmental factors, primarily temperature, and relative humidity[11,12].

[1]UFMG – Universidade Federal de Minas Gerais, Faculdade de Engenharia, Departamento de Engenharia de Estruturas, Av. Pres. Antonio Carlos, 6627, 31270-901, Belo Horizonte - MG, Brazil

[2]Supmicrotech-ENSMM, CNRS, FEMTO-ST, Département Mécanique Appliquée, UBFC - Université de Bourgogne Franche-Comté, Besançon, France

[3]UNESP – Universidade Estadual Paulista, Faculdade de Engenharia de Ilha Solteira, Departamento de Engenharia Mecânica, Ilha Solteira, Brazil

[4]Faculty of Engineering, Lusófona University, Campo Grande 376, 1749-024 Lisboa, Portugal

[5]CERIS, Instituto Superior Técnico, Universidade de Lisboa, Av. Rovisco Pais 1, 1049-001 Lisboa, Portugal

[6]IDMEC, Instituto Superior Técnico, University of Lisbon, Portugal

Corresponding author:
Carlos Cimini, UFMG – Universidade Federal de Minas Gerais, Faculdade de Engenharia, Departamento de Engenharia de Estruturas, Av. Pres. Antonio Carlos, 6627, 31270-901, Belo Horizonte - MG, Brazil.

A comprehensive exploration of Lamb wave theory, its experimental implementations, and its significance in SHM is delivered by Mitra et al.[13].

Among the various network architectures utilized for Lamb wave signal analysis, CNNs have gained prominence in recent years[14,15]. CNNs are a feed-forward ANN architecture consisting of layers that alternate between convolutional and sub-sampling operations. They excel in detecting patterns in input data with minimal preprocessing required before input. Consequently, they are categorized based on the type of input layer they use. In the case of 2D networks, bi-dimensional arrays, such as images, serve as the input, whereas in uni-dimensional networks, 1D arrays, such as time series, are employed. Both networks can handle input signals with multiple parallel channels, such as RGB (Red, Green, and Blue) channels in images or multiple parallel series in the case of 1D time series. Several studies have proposed using CNNs for Lamb wave analysis, focusing on 2D networks.[14–17].

However, one major limitation of using 2D CNNs in Lamb wave applications is the requirement to convert the temporal signals to 2D arrays using some algorithms, e.g., Continuous Wavelet Transform[16]. In contrast, 1D CNNs have the advantage of working directly with the time series data of Lamb waves, eliminating the need for hand-crafted features or applying transformation algorithms. Recent works have used variations of 1D CNN architecture to analyze raw discrete time-domain Lamb waves and detect damage on thin metallic plates[18–23] and on composite structures[24,25]. Kyraniaz et al.[26] presents a comprehensive discussion about 1D CNN structures and applications.

The reliability of a machine learning algorithm is limited by the amount and quality of the data utilized in its training stage. As it is not feasible to intentionally damage most structures and measure their behavior under all potential damage scenarios and environmental conditions, even in laboratory settings, creating specimens with predetermined and characterized damage types and locations is impractical. Conversely, when machine learning algorithms are trained with limited data, their ability to generalize on unseen data after the training stage may be compromised. To overcome this, hybrid training strategies integrate supplementary data derived from physics-based restrictions and/or mathematical models into the training process of machine learning algorithms[27,28].

Modeling guided wave propagation in composite structures is an intense field of research, and several methods are available in literature[29,30]. The FE method stands out among available approaches due to its relative ease of implementation and commercial codes with extensive element libraries readily available. As the FE method assumes a full 3D displacement field, it can accurately capture the wavefront propagation in complex structures[31]. These methods usually have a very fine mesh density to simulate high-frequency signals or small model features on the structure. They are updated with experimental data (when available) to account for environmental conditions' variations and address experimental dispersion. FE model updating techniques can be categorized into deterministic and stochastic (or probabilistic) approaches[32]. Deterministic updating approaches involve formulating a minimization problem and seeking optimal values for physical parameters. Several authors have used deterministic FE models to replicate and produce Lamb wave data for SHM purposes. These works usually consider or define a value or range of values for numerical properties and add stochastic noise to address measurement variations[20,33–36]. Contrarily, Bayesian inference can be used to gather information about a posterior probability distribution of model parameters based on prior knowledge, experimental data, and a likelihood function and account for uncertainty in the model's predictions. The advantage of this approach is to directly incorporate the variability of experimental data into the numerical model to render it stochastic. The Bayesian updating framework has been extensively used in damage detection, model updating, and system identification[37–41]. Previous studies have applied Bayesian inference to composite structures subjected to Lamb wave excitation, using methods like LISA and Wave and Finite Element assisted surrogate models[42,43], and Ferreira et al.[44] used Bayesian inference to update a FE model using a neural network surrogate model.

This paper introduces a novel data-driven methodology for monitoring the condition of composite structures using Lamb waves, employing a 1D CNN trained on data sourced from a Bayesian stochastic FE model. It represents the effort to utilize data from a Bayesian-calibrated FE model specific to Lamb wave propagation for training a machine learning model to assess damage in composite structures subjected to variable temperatures. The Bayesian inference updates the FE model in restricted experimental data, deploying a Markov-Chain Monte Carlo (MCMC) technique combined with the Metropolis-Hastings sampling algorithm. Throughout this updating procedure, surrogate models built on MLP neural networks are leveraged to decrease the computational time demanded by the MCMC iterations. Opting for a stochastic FE model to create training data has multiple benefits: it reduces the experimental requirement for a damage quantification algorithm development, accelerates the training process, and can boost accuracy in data-scarce scenarios by providing a richer dataset for learning. Harnessing the broad generalization abilities of machine learning algorithms and the statistical sense of Bayesian inference for model adaptation, a stochastically updated model emerges as a sturdy data foundation for training machine learning SHM algorithms. By integrating insights from the stochastic FE model during training, the machine learning algorithm can exploit the FE model's inherent uncertainty and generalize across unobserved experimental data. This methodology empowers a 1D CNN to discern core characteristics from the FE model, thus enhancing its predictive accuracy, particularly when trained on a limited experimental dataset.

The effectiveness of the suggested framework is gauged across three distinct training contexts: exclusive experimental data, purely numerically generated data, and a combined set of experimental and numerical data. This paper proposes

two significant contributions. First, it outlines the forging of a Bayesian data-driven machine-learning technique, drawing from a stochastic FE model, to quantify damage magnitude in composite structures under fluctuating temperatures. Second, it delves into the interplay between experimental and numerical data on the performance of a 1D CNN architecture regarding both confidence intervals and prediction quality.

The structure of this paper is as follows. Section Problem statement and theoretical background provides an overview of the proposed framework, including the relevant theoretical background. Section Methodology details the experimental setup, the FE model, the surrogate modeling strategy, and the datasets utilized during the 1D CNN training rounds. Subsequently, in section Results, Bayesian inference is applied to update the FE model, the hyperparameters of the 1D CNN are tuned, and the proposed Bayesian data-driven machine learning strategy is evaluated in terms of accuracy and the impacts of temperature variations. Finally, section Discussions engages in discussions about the results, while section Conclusions presents the final remarks and suggests potential directions for future research

Problem statement and theoretical background

This section describes the main parts of the proposed Bayesian data-driven framework to quantify damage size on a composite structure. The proposed framework consists of two parts i) stochastic FE model development and ii) 1D CNN training and evaluation. Fig. 1 presents the proposed framework used for this work. The first step comprises a stochastic updating of a FE model using Bayesian inference through MCMC simulations with the Metropolis-Hastings sampling algorithm. A sensitivity analysis using Sobol indices and a surrogate modeling strategy defines the relevant parameters and speeds up the MCMC rounds. Following the updating process, a 1D CNN is trained with datasets from three different strategies: (i) only experimental data, (ii) only numerical data, and (iii) a hybrid combination of both. The proposed 1D network is applied after a binary classification to assess the presence or absence of damage[45,46] Therefore, it does not evaluate the structure in a damage-free situation, it is used to quantify damage in a scenario in which damage is already detected. Section Experimental setup expands this discussion.

The proposed framework is grounded on the following assumptions and considerations:

1. The experimental dataset made available by da Silva and Paixao[47] is used as an experimental setup, and it is considered that no material property is known *a priori*.
2. The experimental database is divided into training and test datasets. The test dataset is used only at the end to evaluate the performance of the machine learning algorithms.
3. The training dataset is used to update the material properties of a FE model, using the framework proposed by Ferreira et al[44].
4. The FE model accounts for the experimental results variability through variations in material properties; therefore, there is not a unique value for a given property. Instead, there is a Probability Density Function (PDF) for each significant parameter.
5. A Bayesian inference process using MCMC simulations and the Metropolis-Hasting sampling algorithm is effective in sampling posterior PDFs from uniform prior distributions.
6. The FE model can be used to simulate other conditions inside and outside the range of damages in which it is calibrated.
7. A surrogate model, based on neural networks, can replace the FE model to reduce the time required for the MCMC rounds.
8. A 1D CNN is implemented to quantify damage in a structure with detected damage.
9. A 1D CNN can gather features of the raw data series. It can be trained using experimental data, numerical data, or a hybrid combination of both, comprising three different types of datasets.
10. The proposed strategy is evaluated by comparing the performance of machine learning algorithms trained in the three types of datasets.
11. The network performance is evaluated using a test dataset not used during the Bayesian inference process or the training stage.

Stochastic FE model development

This work uses the Bayesian updating framework proposed by Ferreira et al.[44] to obtain a stochastic FE model for Lamb wave propagation under varying temperatures. Figure 2 presents the proposed strategy, divided into two main steps: an initial deterministic updating step and a stochastic updating procedure. The deterministic updating is based on a variation of the least-squares method. In contrast, the stochastic updating procedure is composed of a sensitivity analysis using Sobol indices followed by an MCMC simulation using the Metropolis-Hastings sampling algorithm to sample the posterior probability function of the main parameters of the model, i.e., those that influence the model output the most. The framework is applied for multiple temperatures, enabling the construction of a model capable of emulating a complete experimental dataset across a range of temperatures.

- *Deterministic updating procedure.*

A modified variant of the least-squares method is employed for the deterministic updating of input parameters. The formulation of this method is detailed by Bud et al.[48], and it displays a multi-loss optimization technique designed to minimize several loss functions derived from model outputs. To realize this goal, the influence of each

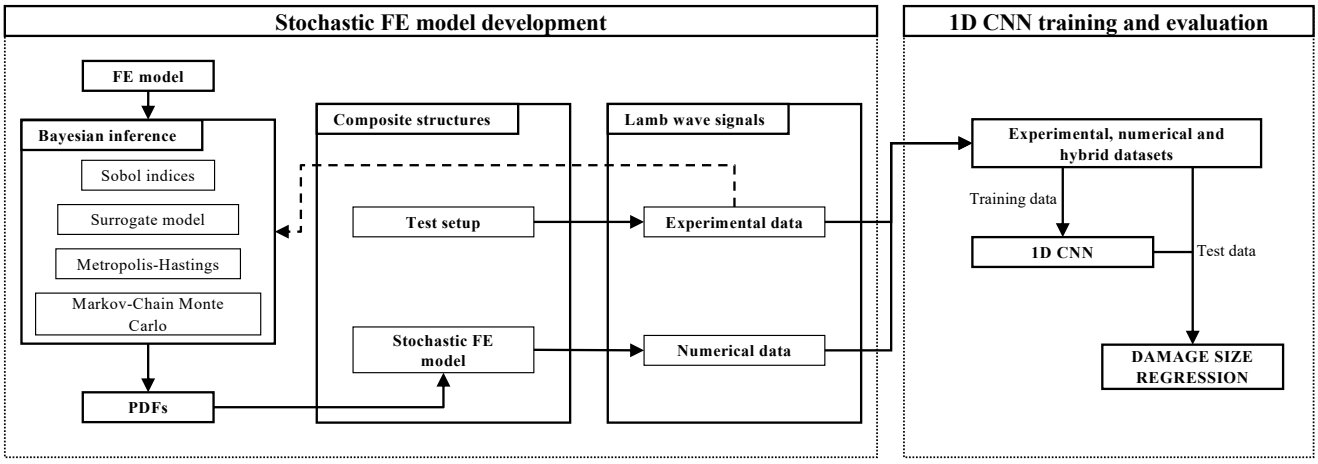

Figure 1. Proposed Bayesian-driven framework for stochastic FE model updating, data generation, and machine learning algorithm training and evaluation.

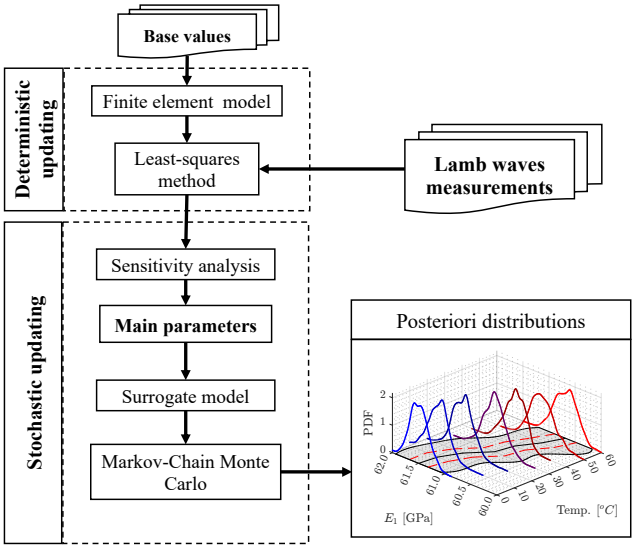

Figure 2. Stochastic FE model updating process.

input parameter on the loss functions is linearized, and partial derivatives relative to each parameter are numerically computed. Two residuals are established as loss functions: the squared norm of the disparity between experimental and numerical signals and the cross-correlation between the signals. Table 1 elucidates the definitions of both residuals. It is important to highlight that while the equations provided appear continuous, they are executed through discrete numerical computations. The aggregate residual is characterized as the summation of the individual residuals.

Residual	Equation
R_{NORM}	$R_{\text{NORM}} = \dfrac{\int_{t_1}^{t_2} [y(t) - x(t)]^2 dt}{\int_{t_1}^{t_2} x(t)^2 dt}.$
R_{XCOR}	$R_{\text{XCOR}} = 1 - r_{xy},$

Table 1. Residuals used in the updating process

- *Sobol indices*

Sensitivity analysis is conducted to discover the effects of model parameters, called random input variables, on quantities of interest that form the model response. A sensitivity analysis is performed using Sobol indices to quantify each parameter's influence on the model's behavior. The model parameters are perturbed within a defined range, and metrics defined to quantify the input parameters' effect on the model's response are evaluated. The first-order Sobol index measures the proportion of variance in the metrics that can be attributed to a single parameter.

Suppose the response of the mathematical model is given by:

$$Y = \mathcal{M}(\boldsymbol{\Theta}), \tag{1}$$

where $\boldsymbol{\Theta} = (\theta_1, \theta_2, \ldots, \theta_k)$ is the vector containing the k input variables, and Y is a scalar quantity. For simplification purposes, the input parameters are considered uniformly distributed with support $\pi(\boldsymbol{\Theta}) \sim \mathcal{U}(0, 1)$. The sensitivity analysis using Sobol indices considers the decomposition of the model's response Y in terms of increasing dimensions:

$$Y = \mathcal{M}_0 + \sum_{i=1}^{k} \mathcal{M}_i(\theta_i) + \sum_{i<j}^{k} \mathcal{M}_{ij}(\theta_i, \theta_j) + \ldots + \mathcal{M}_{1\ldots k}(\theta_1 \ldots \theta_k), \tag{2}$$

where the constant $\mathcal{M}_0$ corresponds to the mean value $E(Y)$ of the model output. The integral of each summation above has zero means, then all the terms in Eq. (2) hold the orthogonality property. Consequently, these terms can be calculated using the conditional expectations $\mathcal{M}_0$. Thus, the terms $\mathcal{M}_i(\theta_i)$ and $\mathcal{M}_{ij}(\theta_i, \theta_j)$ are the conditional mean values for the parameters i and ij $(i \neq j)$[49], respectively:

$$\mathcal{M}_i(\theta_i) = \int_0^1 \cdots \int_0^1 \mathcal{M}(\boldsymbol{\Theta})\ d\boldsymbol{\Theta}_{\sim i} - \mathcal{M}_0, \tag{3}$$

$$\mathcal{M}_{ij}(\theta_i,\theta_j) = \int_0^1 \cdots \int_0^1 \mathcal{M}(\boldsymbol{\Theta})\ d\boldsymbol{\Theta}_{\sim ij} - \mathcal{M}_0 - \mathcal{M}_i(\theta_i) - \mathcal{M}_j(\theta_j), \tag{4}$$

where the notation $\sim i$ indicates that parameter θ_i is excluded. As the model response from Eq. (1) is also a random variable, the conditional expectation variance can be considered a summary measure of sensitivity. Thus, one can compute the first-order Sobol indices that quantify the additive effect of each input parameter separately on the total variance:

$$S_i = \frac{Var[\mathcal{M}_i(\theta_i)]}{Var[\mathcal{M}(\boldsymbol{\Theta})]}, \tag{5}$$

This first-order index represents each input parameter's main contribution to the model output variance[50]. The second-order Sobol indices that quantify the interaction effects between two input parameters are defined as:

$$S_{ij} = \frac{Var[\mathcal{M}_{ij}(\theta_i,\theta_j)]}{Var[\mathcal{M}(\boldsymbol{\Theta})]}. \tag{6}$$

In this work, the first and second-order Sobol indices are analyzed to evaluate the influence of each input parameter in the FE model response. For this, the UqLab framework has been used[51]. Two metrics are defined based on the Lamb wave package, as depicted in Fig. 3: (i) the time of flight (TOF), and (ii) the maximum amplitude of the wave package.

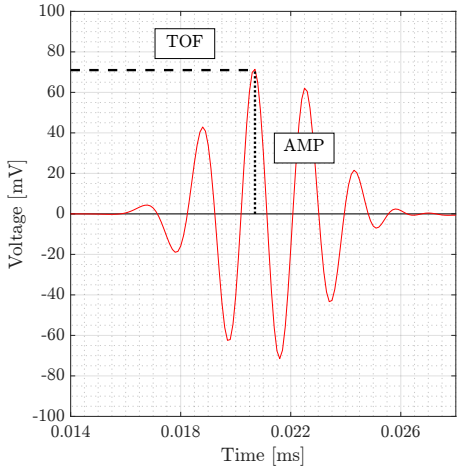

Figure 3. Metrics used at sensitivity analysis

- *Bayesian inference*

Due to the intrinsic variability present in physical systems, such as variations in geometry, environmental conditions, and material properties, it is impossible to eliminate uncertainty, even with comprehensive data. This type of uncertainty, irreducible uncertainty, cannot be fully captured or accounted for. To address this variability in the parameters of the computational model, this study employs the Bayesian paradigm as a statistical inference tool for the problem of model calibration. Bayesian inference is a probabilistic framework that allows for the iterative updating of prior beliefs about a model or hypothesis based on observed data. It involves the application of Bayes' theorem, which describes the mathematical relationship between prior knowledge, a likelihood function, and the posterior distribution. The prior distribution defines the initial beliefs, or knowledge, about the system of interest; the likelihood functions quantifies the probability of observing data given different input parameters; and the posterior distribution combines the prior and the likelihood to provide an updated belief about the model. Using Bayesian inference, it is possible to incorporate new evidence in the model. It also facilitates the quantification of uncertainty in model parameters through PDFs.

In a Bayesian inference process, two assumptions are introduced: (i) as the model parameters are random variables, a prior distribution $\pi(\boldsymbol{\Theta})$ for the set of input variables $\boldsymbol{\Theta}$ is proposed based on the deterministic model updating procedure; (ii) Bayes' theorem is employed to update the before a posterior distribution, gathering information from random data observations ($\mathscr{D}$). The posterior PDF $\pi(\boldsymbol{\Theta}|\mathscr{D})$ is given by:

$$\pi(\boldsymbol{\Theta}|\mathscr{D}) = \frac{\pi(\mathscr{D}|\boldsymbol{\Theta})\pi(\boldsymbol{\Theta})}{\pi(\mathscr{D})}, \tag{7}$$

in which $\pi(\mathscr{D}|\boldsymbol{\Theta})$ is the likelihood function and the denominator $\pi(\mathscr{D})$ is the marginal, a normalization constant that guarantees the definition of a PDF with integral equal to unity. By considering a uniform prior distribution, Eq. (7) is simplified to $\pi(\boldsymbol{\Theta}|\mathscr{D}) \propto \pi(\mathscr{D}|\boldsymbol{\Theta})$, i.e., the updated posterior PDF is proportional to the likelihood distribution.

Assuming that the model predictions $\mathcal{D}^{\mathcal{M}}(\boldsymbol{\Theta})$ are corrupted by an additive decorrelated Gaussian noise of zero mean and variance σ_ε^2, the analytical expression for the likelihood function is given by:

$$\pi(\mathcal{D}|\boldsymbol{\Theta}) \propto \exp\left(-\frac{1}{2}\frac{\left(\mathcal{D}-\mathcal{D}^{\mathcal{M}}(\boldsymbol{\Theta})\right)^T\left(\mathcal{D}-\mathcal{D}^{\mathcal{M}}(\boldsymbol{\Theta})\right)}{\sigma_\varepsilon^2}\right), \tag{8}$$

with T superscript meaning transpose operation. To sample the posterior density function, the MCMC/Metropolis-Hastings algorithm is considered[52]. The random variables $\boldsymbol{\Theta}$ are limited to the interval $[\boldsymbol{\Theta}_{\min}, \boldsymbol{\Theta}_{\max}]$, whose current state is symmetrically normalized as $\boldsymbol{\Theta}' = (1-\boldsymbol{x})\boldsymbol{\Theta}_{\min} + \boldsymbol{x}\boldsymbol{\Theta}_{\max}$; $\boldsymbol{x}$ is a random variable $\in [0,1]$ that represents generated candidates for the posterior distribution. These candidates are sampled from a normal distribution with standard deviation σ_p. This hyperparameter controls the random walk step to avoid the chain becoming static and, simultaneously, to allow the parameter space to be properly explored. Therefore, σ_p is adjusted to obtain an acceptance rate of candidates from 40 to 50 %. Only 80% of the Monte Carlo simulations are considered in the final stationary Markov chain (burn-in of 20%).

Overview of neural networks

In this work, two architectures of neural networks are used, the MLP and the CNN. The former is used as a surrogate

model instead of the FE model, while the latter is used as a regression algorithm.

Multilayer perceptron MLP consists of a series of interconnected layers of neurons that receive the information from the previous layer neurons, process it then pass it forward. Assuming a training dataset with dimension $M \times N$, where M is the number of points per array, and N is the number of samples on the dataset, the l-th sample vector is represented by $\boldsymbol{x}^{(l)} \in \mathbb{R}^{1\times M}$. In a supervised learning scheme, the expected output for a training sample is represented by $\boldsymbol{y}^{(l)} \in \mathbb{R}^{P\times 1}$, where P is the number of outputs. The objective of the neural network is to map the function $\mathcal{F} : \boldsymbol{x}^{(l)} \rightarrow \boldsymbol{y}^{(l)}$. A neural network with at least one hidden layer can act as a universal approximator[53] and Fakih et al.[54] demonstrated the feasibility of neural networks as a surrogate model to simulate Lamb waves in aluminum structures.

This mapping is achieved through the training process, in which the parameters $\boldsymbol{\Theta}_{NN}$ of the network are updated using a set of sample pairs $(\boldsymbol{X}^{(l)}, \boldsymbol{Y}^{(l)})$ through a minimization problem of a loss function $\mathcal{L}(\boldsymbol{\Theta}_{NN}) = \mathcal{L}(\boldsymbol{\mathcal{F}}(\boldsymbol{X}, \boldsymbol{\Theta}_{NN}) - \boldsymbol{Y})$. The half-mean-squared error is used as a loss function in regression problems.

Considering the kth unit (or neuron) of the ith layer, it receives the output x_{ij} from each jth unit of the (i-1)st layer. The values x_{ij} are then multiplied by a weight w_{ijk}, and these products are summed. A bias b_{ij} is added to the result, and then an activation function ($\boldsymbol{\mathcal{T}}$) is applied to the result that is propagated for the next layer. The activation function is responsible for adding non-linearity to the system, and it can assume multiple forms, such as sigmoid, ReLU, leaky ReLU, or $tanh$ functions.

$$\boldsymbol{x}_{i+1,k} = \boldsymbol{\mathcal{T}}\left(\sum_{j=1}^{m} w_{ikj}x_{ij} + b_{ij}\right). \tag{9}$$

The training stage involves feeding the network with labeled input data and adjusting its internal parameters to minimize the difference between predicted outputs and true labels. As this process consists of a multivariate optimization, $\boldsymbol{\Theta}_{NN}$ is not necessarily unique and can produce multiple networks that fit the data. To encode the preference for certain sets of weights and remove part of this ambiguity, it is common to add a regularization loss in the form of: $\mathcal{R}(\boldsymbol{\Theta}_{NN}) = \lambda \sum_i \sum_j (\boldsymbol{\Theta}_{NN})_{ij}$, in which λ is a regularization parameter. This is commonly called L_2 regularization, and it induces the optimization algorithm to select models with smaller parameters. This regularization strategy also impacts reducing overfitting, as highly specialized networks, with concentrated parameters are penalized over the ones with a more uniform weight distribution. A forward propagation stage generates the predicted output throughout the training process, subsequently compared to the actual output to calculate the loss. Backpropagation is then performed to update the network parameters by computing gradients and applying optimization algorithms. This process is iterated for multiple epochs involving forward pass, loss calculation, backpropagation, and parameter updates. Finally, the trained network is evaluated on a test set to address its performance.

Convolutional neural network CNNs have a significant advantage over traditional ANNs because they can integrate feature extraction and classification tasks within a single framework. Unlike conventional machine learning approaches that often involve preprocessing steps and rely on hand-crafted features, which can be sub-optimal and computationally demanding, CNN-based methods directly extract "learned" features from raw data, thereby maximizing accuracy. Kiranyaz et al.[55] presents an extensive discussion about 1D CNN and exemplifies this network structure with various applications. In the field of SHM using Lamb waves, Shao et al.[19] proposed a multi-level damage classification technique of aircraft plate-type structures using a 1D-CNN. Rai and Mitra[18] introduced a multi-headed 1D-CNN and evaluated a transfer learning strategy using a deterministic 2D FE model and two similar AL-5052 plates. Pandey et al.[20] employed the Local Interpretable Model-Agnostic Explanations (LIME) with a 1D CNN to interpret the classifications of the model in terms of damage feature contributions.

A CNN performs a similar mapping $\mathcal{F} : \boldsymbol{x}^{(l)} \rightarrow \boldsymbol{y}^{(l)}$ as described for the MLP network, but it uses a sequence of convolution and pooling operations. The first step is the convolution operation, where a filter or kernel is convolved with the input feature map. This operation can be represented mathematically as $Y = X * W$, where Y is the output feature map obtained by convolving the kernel W with the input X. After the convolution operation, an activation function is applied element-wise to introduce non-linearity, resulting in an activated feature map Z. The next step in a CNN is the pooling operation, which helps reduce the spatial dimensions of the feature map while preserving important information. Max pooling and average pooling are commonly used pooling operations, where the maximum value and the average within a pooling window are selected, respectively. Multiple convolution+pooling layers are usually applied in sequence to extract features with increasing complexity from the input. Along the network, normalization layers, such as Batch Normalization, can be used to normalize the activations within a layer to address the problem of internal covariate shift. By normalizing the activations, normalization layers help stabilize and regularize the learning process, enable faster convergence, and improve the network's generalization ability. Also, a dropout layer can be applied to randomly drop some neurons during training to zero. The main purpose of dropout is to prevent overfitting and improve the generalization performance of the network. By dropping out neurons, dropout layers help create a more robust network that avoids relying too heavily on specific connections. At the end of the network, the pooled feature map is flattened and fed into one or more fully connected layers, similar to an MLP network, and the output layer of the CNN applies an activation function

suitable for regression. Figure 4 depicts the 1D CNN used for quantification.

This study utilizes 1D CNNs as quantification algorithms trained with three distinct datasets: (i) an experimental dataset representing a data-driven approach; (ii) a dataset comprising exclusively numerically generated data; and (iii) a dataset that combines experimental and numerical data obtained from a stochastic numerical model.

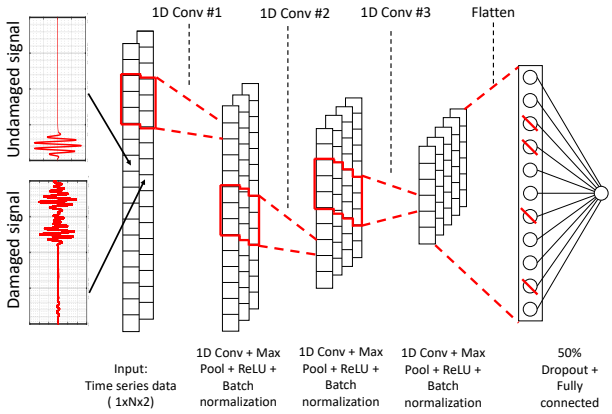

Figure 4. Structure of the 1D CNN used for damage quantification.

Methodology

Experimental setup

The carbon fiber reinforced polymer (CFRP) plate used in the experimental setup has dimensions of 500 x 500 x 2 mm and comprises 10 layers of plain weave fibers oriented along the plate borders directions. To detect the behavior of the plate, four PbZrTi (Lead Zirconate Titanate - PZT) SMART Layers with a diameter of 6.35 mm are bonded to the plate with the help of epoxy resin. PZT 1 acts as the actuator, and the remaining PZTs, namely PZT 2, PZT 3, and PZT 4, serve as sensors. The excitation signal consists of a 5-cycle sinusoidal wave with an amplitude of 35V and a frequency of 250 kHz, modulated by a Hanning window. The output signal is then recorded over a 100 μs window using a multi-function input/output device NI USB 6553 from National Instruments and an oscilloscope DSO7034B from Keysight with a sampling frequency of 5 MHz. Figure 5a presents the experimental setup. The data acquisition is conducted under controlled temperatures, which are incrementally increased in steps of 10°C from 0°C to 60°C, using a thermal chamber manufactured by Thermotron. The data is statistically characterized by performing 100 repeated tests at each temperature. The dataset is publicly available in the GitHub* repository CONCEPT: CarbON-epoxy CompositE PlaTe[47].

Damage is simulated by adding mass to the plate, with increasing diameter, ranging from 20 to 80 mm, with increments of 10 mm. This mass addition simulates local variation on the damping of the plate[56] and allows reversibly simulating damage. Overall, the dataset comprises 28 damaged conditions. Figures 5b to 5e show one experimental measurement for each temperature from 0°C to 60°C and diameter from 20 to 80 mm. Note in Figs. 5b to 5e that the effect of damage is primarily the reduction of the waveform amplitude. This reduction is temperature-dependent, being more pronounced at low temperatures than at high temperatures (refer to Figs. 5b and 5e). Conversely, the temperature alone slightly influences the signal TOF[46], which can be seen comparing the outer signals from the refered figures. Thus, determining whether this structure has damage or not is summarized as an assessment of the signal amplitude with respect to the baseline, which can be implemented with an outlier detection. The difficulty of this problem lies in quantifying the size of the damage, due to the temperature influence in the signal attenuation related to damage. Thus, the proposed 1D CNN is assumed to be applied after a binary classification (presence or absence of damage), and it does not evaluate the structure in a damage-free situation.

Although representing a vast sample space of 0 to 60°C and 20 to 80 mm, the database under study has few samples, making it difficult to divide the data classically, such as fractions of 70/15/15 or 80/10/10 for training, validation, and testing, respectively. Divisions like these would result in validation and test subsets with only 3 or 4 elements, which makes it challenging to evaluate machine learning algorithms during training and testing. Additionally, the authors decided against using K-fold cross-validation to ensure that there is a dataset that the model has never encountered before. In the present work, it is proposed to evaluate the gain of information from a stochastic FE model filling the sample space with generated data under conditions of sparse experimental data and the advantages of the proposed Bayesian framework in these situations. To comprehensively evaluate the performance of the proposed Bayesian framework, the experimental data is arranged into a scenario in which data could be feasibly collected at various temperatures with minimal cost in a practical scenario, as depicted in Tab. 2. This division simulates a common laboratory situation in which the structure could be damaged in limited conditions and tested at several temperatures. This database allows for the evaluation of temperature interpolation capacity in two ranges with different sizes - from 10 to 30°C and from 30 to 60°C, as well as the analysis of damage interpolation capacity between 30 and 70 mm, and the study of the extrapolation capacity with damages of 20 and 80 mm.

FE model

An ABAQUS/Explicit FE model is used to simulate the plate. The plate is modeled using continuum shell elements (SCR8). These elements are designed to discretize a three-dimensional body rather than just representing a surface like traditional shell elements. Continuum shells solely possess

*https://github.com/shm-unesp/DATASET_PLATEUN01

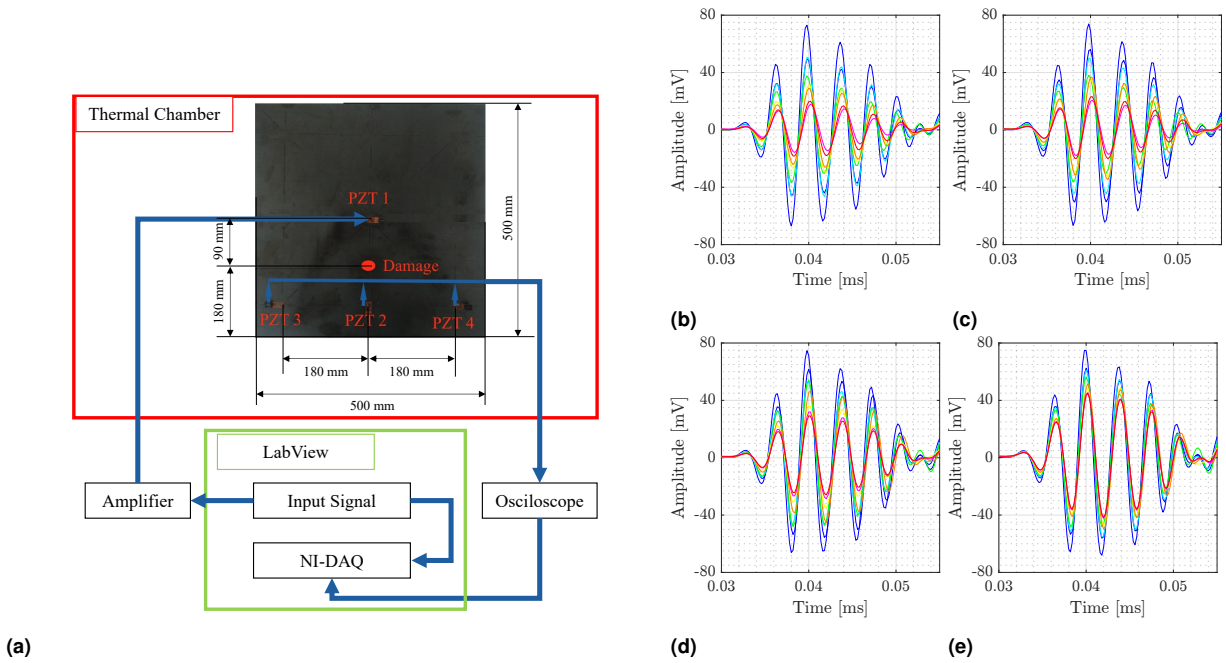

Figure 5. Experimental setup: (a) data acquisition strategy; and results for progressive damaged conditions from 20 mm to 80 mm at (b) 0°C; (c) 10°C; (d) 30°C; and (e) 60°C.

Damage diameter [mm]	Temperature [°C] 0	10	30	60
0				
20				
30				
40				
50				
60				
70				
80				

Table 2. Data division between training (), validation (), test (), and undamaged ()

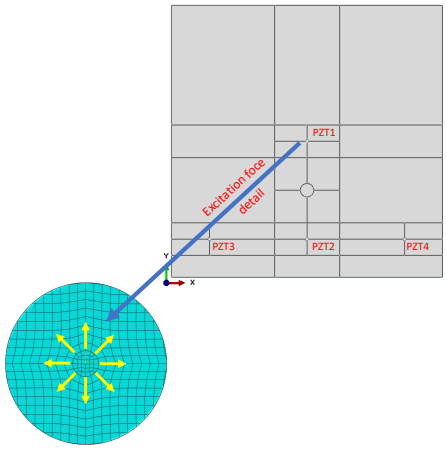

Figure 6. FE model.

displacement degrees of freedom, adopt linear interpolation, and account for the impact of transverse shear deformation and thickness alteration. Furthermore, they are founded on first-order composite theory and can be stacked to enhance the precision of the through-thickness response.

Figure 6 presents the geometry of the FE model. To facilitate the generation of a structured mesh for the entire plate, the plate is divided into several smaller rectangular regions. The area where the PZT actuators and sensors are attached to the plate is modeled explicitly with a circular mesh. As proposed by Gresil et al.[57], the excitation signal is applied as eight self-balancing forces around this region, as depicted in Fig. 6. To obtain the output signal, the integrated strain results within the sensor region are used and transformed to voltage as suggested by Sirohi, and Chopra[58]. The region between PZTs 1 and 2 is modeled with a circular mesh to account for damage addition. Damage is modeled as a constant thickness circular disk with solid elements and a tie interaction with the plate.

The analysis's spatial and temporal resolution influences the numerical simulation's stability. Moser[59] suggests that a spatial resolution of no less than 20 nodes per wavelength is essential to guarantee stability, which can be expressed as $l_e = \lambda_{min}/20$, where λ_{min} is the minimum wavelength anticipated in the model and l_e is the characteristic length of the mesh. Furthermore, to avert numerical instability, the time step must be determined based on the highest anticipated frequency in the simulation, with a suggested value of $\Delta t = 1/(20 f_{max})$, where Δt represents the time step and f_{max} denotes the maximum frequency expected in the model. When the input frequency is 250 kHz, adhering to both considerations leads to a mesh comprising element sizes of approximately 2 mm and a maximum time increment of 0.2 μs. However, further stability analyses of the model reveal that the time increment of 0.2 μs is not sufficient to ensure convergence, due to mesh irregularity surrounding the damage and PZT regions. Additionally, reducing the time increment to 0.10 μs allows the model to converge in most

simulations, but divergence occurs in some combinations of properties resulting in faster wave speeds. Fig. 7 presents the results of a simulation with time increments of 0.10 μs, 0.075 μs, 0.05 μs, 0.04 μs, 0.03 μs, and 0.02 μs. Note that the model results on Fig 7a are very similar. Additionally, the TOF of the signal on Fig. 7b with a time increment of 0.05 μs, but the simulation duration increases exponentially with the increment. Consequently, a time increment of 0.05 μs is selected because it effectively addresses mesh irregularities, ensures convergence in all simulated scenarios, and maintains a reasonable simulation duration.

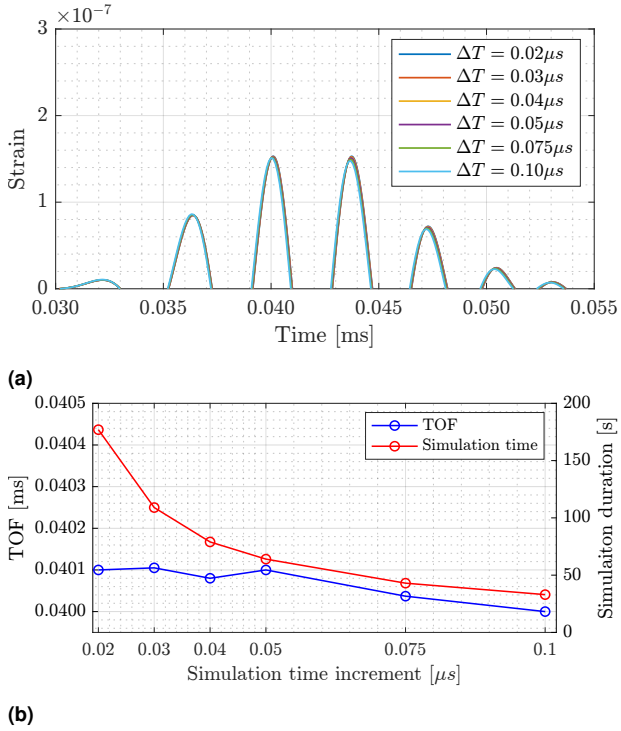

Figure 7. Convergence analysis of the FE model as a function of the time increment : (a) wave packets, and (b) TOF and simulation duration.

The composite material is implemented in the FE model using ply-based properties. The mechanical behavior of the materials is modeled using the classical laminate theory, where each layer is considered an orthotropic material with 3 integration points per lamina. As such, Young's modulus in two perpendicular directions in the plane (E_1 and E_2), Poisson's ratio (ν_{12}), shear moduli in and out of the plane (G_{12} and G_{23}, respectively), and density (ρ) had to be determined. As a simplification, it is assumed that the values of E_1 and E_2 for plain weave fibers are close, so they are considered equal. The emulated damage mass is modeled as an elastic material with Rayleigh damping, characterized by two coefficients, α and β (Eq. 10). It can be observed that in Rayleigh's damping, α predominates at low frequencies, while β dampens high frequencies

$$\xi = \frac{\alpha_R}{2\omega} + \frac{\beta_R \omega}{2}. \tag{10}$$

The model accounts for temperature effects at the material level. Initially, the elastic modulus in perpendicular directions (E_1 and E_2), Poisson's ratio (ν_{12}), and shear moduli in and out of the plane (G_{12} and G_{23}) are heuristically selected as factors affected by temperature for the composite material. The Young modulus, Poisson coefficient, and Rayleigh damping coefficients (α and β) are considered temperature-dependent for the damage mass simulation material. The specific mass of both materials is considered constant with temperature but treated as an uncertain quantity for both materials.

The FE model is implemented using a series of Python routines that run within the ABAQUS Compiler. This setup allows for the generation of parametric plate geometry, creation of damage, and definition of the mesh. Additionally, there exists a high-level code layer implemented in MATLAB, providing direct control over Abaqus through the MATLAB command line. The primary command function, denoted as the main model in Fig. 8, integrates the property generation routine, i.e., deterministic and stochastic routines. The output is a trigger file written in Python. Through a Windows system command, MATLAB commands ABAQUS to construct the structure and generate a standard INP file. This file is then interpreted by the ABAQUS Solver, resulting in an ABAQUS OBD file. Subsequently, this file is interpreted and converted into a text file, which can be stored to build a dataset or read by MATLAB to update properties through an automatic routine. This architecture made possible a complete automation of the pre-and post-processing steps of the simulation inside MATLAB's workspace to facilitate the Monte Carlo simulations.

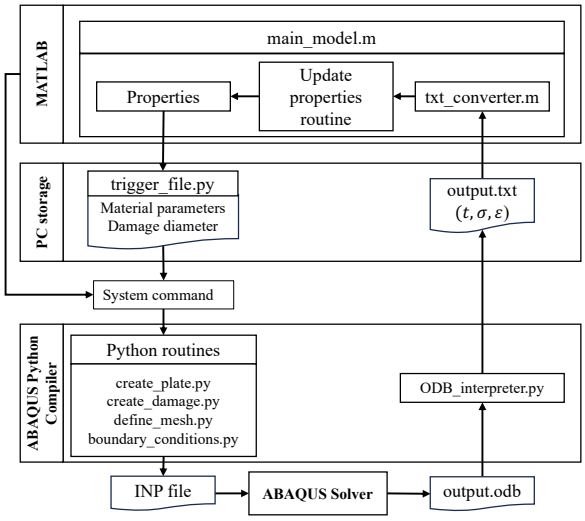

Figure 8. FE model code structure implementation.

Neural network surrogate model

To accelerate the time-consuming MCMC simulations, the authors propose employing a surrogate model to replace the FE-based model during the random-walking process. Numerous surrogate modeling techniques have been suggested to address the computational challenges in Bayesian inference. Some of these techniques include Gaussian process[60,61], polynomial chaos expansion[62,63], radial basis function[64], neural networks[54,65], and others. This

study uses a multilayer perceptron ANN as the surrogate model[44]. It is an interpolation model within the parameters search space for the Bayesian inference process.

The FE model is extensively simulated with properties from a bounded uniform distribution to generate the necessary training data in this strategy. The boundaries are defined by the results of the deterministic updating procedure, which increased by a margin of 5-20%, depending on the uncertainty about the parameter to allow a random-walk margin for the MCMC algorithm. The model response is truncated after the first wave package to reduce training time and data requirements for network convergence. The neural network is trained with the Adam algorithm and uses a dataset division with 80/10/10 proportions for training, validation, and testing sets. The loss of the validation data serves as the stopping criterion for training. The input variables are normalized between 0 and 1 to enhance convergence, while the output signal is normalized between -1 and 1.

The input layer has M neurons representing the random variables updated within the Bayesian inference process, and the output layer contains 140 neurons representing the time series output. The number of hidden layers is defined as two, with the number of neurons N_2 and N_3 at the first and second hidden layers selected through exploratory search. Figure 9 depicts the surrogate model structure.

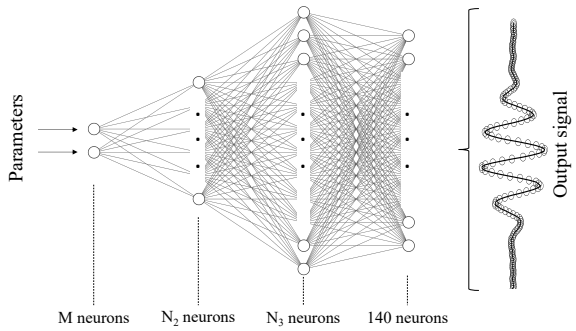

Figure 9. Architecture of the MLP used as surrogate-model.

Results

The results are divided into two subsections (i) the stochastic FE model updating results and (ii) the training and evaluation of the machine learning model. The former is further divided into undamaged and damaged model updating, while the latter is divided into 1D CNN structure definition, damage quantification, and temperature effects.

Stochastic FE model updating

The updating procedure detailed in section Stochastic FE model development is applied to the FE model in the undamaged and damaged conditions. At the undamaged condition, only the plate material parameters are updated (E_1, E_2, ν_{12}, G_{12}, and G_{23}) using experimental data ranging from 0 to 60°C. Conversely, for the damage condition, the emulated damage mass material is updated (E, ν, α, and β) using the available information for 0, 10, 30, and 60°C. Also, the updating procedure of the damage condition only used the experimental signals for diameters of 30, 50, and 70 mm. The other damage diameters are used to evaluate the performance of the proposed damage quantification strategy at the testing phase.

Undamaged model updating The updating process for the undamaged model is presented by Ferreira et al.[44]. Table 3 presents the statistical properties for the mechanical parameters and Figs. 12a to 12h showcases the sampled distributions.

Damaged model updating Evaluating Eq. 10, one can notice that α is responsible for the damping component at low frequencies. Among the available parameters for adjusting the damaged model, initial tests showed that this damping component is insignificant to the model's response. As Lamb waves occur in ultrasonic ranges, specifically 250 kHz for the present study, only β is presented to be relevant. Therefore, the damaged model has four adjustable parameters besides the undamaged model: E, ν, β, and ρ for the damage mass. The initial value of the mass density was determined experimentally as 1750 kg/m^3 and kept constant with temperature. An initial estimate is based on an exploratory search for the other parameters. Table 4 shows the proposed range of values for the parameters of interest. Note that, due to the uncertainty involved in the system, E and β have a wide search range. The Poisson's ratio is limited to 0.45 to avoid potential issues with incompressibility in the FE model.

The updating procedure requires simulating the model with the three training diameters from Tab. 2 (30, 50, and 70 mm) at each parameter alteration. Moreover, adding damping to the system reduces the minimum step required for numerical stability to 0.05 μs. Consequently, the wide range of potential values, combined with multiple damage diameters, significantly increases the computational burden of employing the FE model in an exploratory search strategy. Therefore, an initial sensitivity analysis employing Sobol indices is used. A Latin hypercube strategy with 200 samples is constructed, encompassing the four parameters from Tab. 4 and considering the fixed central damage diameter value of 50 mm. The 30 and 70 damage diameters are not included to keep the model's variance only related to the material properties.

Figure 10 presents the obtained first and second-order Sobol indices. Note that E represents almost 70% of the variance related to the signal's amplitude, complemented by 25% from β. Conversely, the variance of the TOF metric cannot be entirely addressed by individual parameters, as the second-order Sobol indices show that the combination $E\beta$ is responsible for half of this metric variance. The remaining parameters have negligible impact on the model's response; therefore, they are subsequently assigned fixed values, namely 0.4 for the Poisson's ratio and 1750 kg/m^3 for

Table 3. Mechanical parameters obtained for the undamaged model in the temperature range from 0°C to 60°C. Adapted from Ferreira et al.[44]

Parameter	Metric	0°C	10°C	20°C	30°C	40°C	50°C	60°C
E_1	Mean [GPa]	61.46	61.44	61.30	61.06	61.00	60.80	60.67
	Standard deviation [GPa]	0.191	0.207	0.190	0.215	0.195	0.214	0.225
	Coefficient of variation (CV) [%]	0.310	0.337	0.310	0.352	0.320	0.351	0.371
	1% Percentile [GPa]	60.94	60.91	60.82	60.55	60.57	60.20	60.08
	99% Percentile [GPa]	61.98	61.05	61.83	61.67	61.51	61.34	60.32
G_{12}	Mean [GPa]	10.56	10.38	10.26	10.06	10.11	10.01	9.82
	Standard deviation [GPa]	0.116	0.124	0.108	0.114	0.103	0.131	0.121
	Coefficient of variation (CV) [%]	1.09	1.19	1.05	1.14	1.02	1.30	1.23
	1% Percentile [GPa]	10.14	10.06	10.01	9.74	9.84	9.70	9.50
	99% Percentile [GPa]	10.87	10.69	10.55	10.38	10.32	10.40	10.11

Parameter	Minimum value	Maximum value
E [MPa]	100	700
ν	0.35	0.45
1e-7 β	0.5	10
ρ [kg/m^3]	1650	1850

Table 4. Search region for the damaged model parameters.

the mass density. E and β are considered undetermined, and updating their posterior probability distributions is necessary following the Bayesian inference procedure described in section Stochastic FE model development.

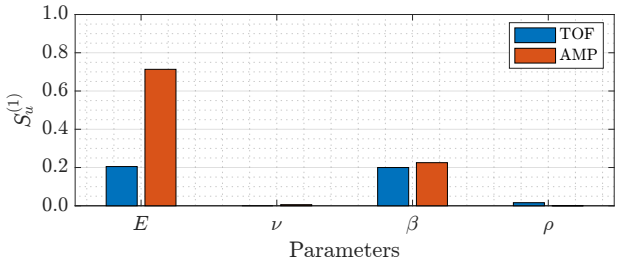

(a)

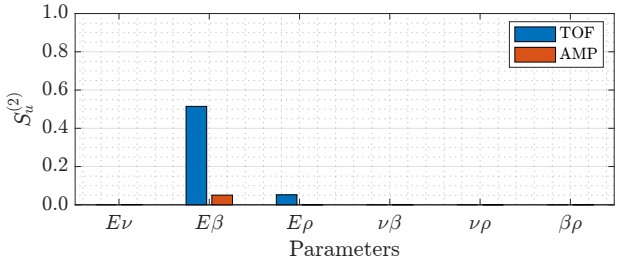

(b)

Figure 10. Sobol indices for the damaged model: (a) first; and (b) second order. TOF (Time of Flight) and AMP (Amplitude)

To perform the MCMC random walks, a surrogate model is proposed[44]. The FE model is simulated multiple times using the uncertain properties sampled from a Latin hypercube bounded by $E \sim (100, 700)$ [MPa] and $\beta \sim 1e^{-7}(0.5, 10)$, along with damage diameters of 30, 50, and 70 mm. Fig. 11 presents the RMSE with respect to the number of neurons in layers 2 and 3, and with respect to the number of samples used in the training phase. Note that the error stabilizes near 0.5% when the second and third layers have 100 and 200 neurons, respectively, and with 576 samples. The selected model has N2 = 100, N3 = 200 and is trained with 1024 samples.

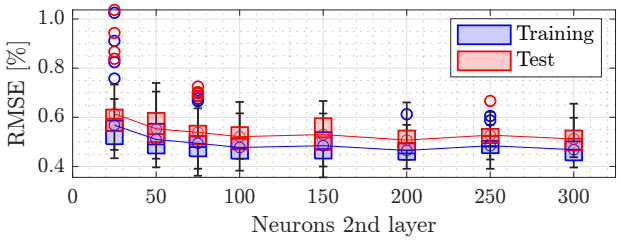

(a)

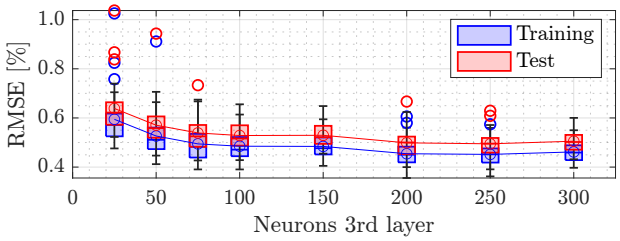

(b)

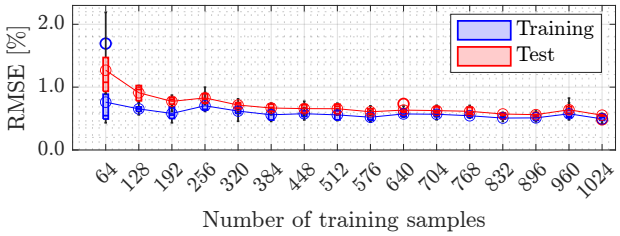

(c)

Figure 11. Surrogate model RMSE in training and test data with respect to: (a) number of neurons in the second layer; (b) number of neurons in the third layer; and (c) samples used in the training phase.

The ANN surrogate model underwent the Bayesian inference process using MCMC with the Metropolis-Hastings algorithm. For the Markov Chain estimation, the variance of the likelihood function is defined iteratively through rounds of the fitting algorithm, trying to ensure a stable acceptance rate between 40 and 50%. The chain is simulated over 4000 samples, and the first 20% samples are discarded (burn-in). Figs. 12a to 12p present the sampled PDFs for E_1, G_{12}, E and β. The PDF is obtained from a kernel density estimate (KDE) applied to the MCMC sampled data. Note that all material properties tend to reduce their magnitude with temperature. Comparing the CFRP and

the emulated damage mass, the latter has a greater variation, with Young modulus and β damping coefficient average values varying from 575 MPa and 3.9×10^{-7} to 475 MPa and 1.5×10^{-7}, respectively.

Samples obtained using the MCMC process are considered a set that approximates the target distribution. These obtained samples are then used as a surrogate PDF representing the target distribution and sample. Simulating the model within its 99% confidence interval for the sampled properties gives the model confidence intervals for the signals, as depicted in Figs. 13a to 13d.

The application of the framework resulted in a Bayesian updated FE model that can be simulated over all ranges of temperatures and provide results with variability within a confidence interval that encompasses the experimental results. The model is a foundation for emulating the experimental setup with and without damage. During the data generation phase, given a temperature, the properties can be sampled from the obtained PDFs. Then, the FE model can be evaluated with the intended damage diameter.

1D CNN evaluation.

In the following subsections, the impact of the data generated by the stochastic FE model in the proposed 1D CNN is evaluated using three different strategies (i) only experimental data, named EXP; (ii) only numerical data, named NUM; and (iii) a combination of both types of data, called hybrid training or HYB. The strategy for each dataset preparation is presented at Datasets preparation, the model's structure is defined in the subsection 1D CNN structure definition, and the data division strategies are evaluated concerning the model's accuracy and temperature effect on sections Damage quantification and Temperature influence.

Datasets preparation The experimental and numerical results must be pre-processed to generate the EXP, NUM, and HYB datasets. The first pre-processing step consists of selecting the first wave package of each k PZT in a damaged condition and concatenating them into a vector $\mathbb{R}^{1\times kN}$. N is defined as 120 points encompassing the FE model's validation region, and k is equal to 3. Therefore, the input signal has a length of $kN = 360$. Then, a reference undamaged signal with dimension $\mathbb{R}^{1\times kN}$ is paired with the damaged signal, creating a sample $\boldsymbol{x}^{(l)} \in \mathbb{R}^{2\times kN}$. Finally, each sample is paired with the scalar damage diameter, also known as severity, represented by $\boldsymbol{y}^{(l)} \in \mathbb{R}^{1\times1}$ and normalized between 0 and 1, considering the range of 0 to 80 mm. The 1D CNN is trained to receive the $\boldsymbol{x}^{(l)}$ array and determine damage diameter $\boldsymbol{y}^{(l)}$ related to it.

The training is performed with the EXP, NUM, and HYB datasets. The EXP dataset is composed only of experimental data. There are 100 experimental signals for each temperature and damage condition of Tab. 2, and the damaged conditions are divided into training, validation, and test subsets according to it. The undamaged signals for each temperature are divided using the same proportion of the damaged conditions, i.e., 2/1/4 and 1/2/4 for 0 and 10°C, respectively. Finally, each damaged signal is permuted with all undamaged signals, expanding the available combination of signals for training, validation, and testing. Table 5 summarizes the data division.

We chose this data partitioning strategy for two primary reasons: (i) Segregating undamaged from damaged signals before distributing them into training, validation, and test datasets ensures entirely distinct subsets. This means no overlap between these subsets, ensuring the neural network is not exposed to test samples during training. (ii) Given experimental uncertainties, two recorded signals under identical conditions are never the same. Consequently, an undamaged baseline can be contrasted with all damaged signals for a specific temperature. By shuffling the baseline within the same temperature bracket, we can diversify available samples for training. For the creation of the NUM and HYB datasets, the numerical signals are procured from the stochastic FE model simulations at temperatures of 0, 10, 30, and 60°C. Diameters are randomly chosen within the range of 20 to 80 mm. Undamaged signals are sourced by sampling PDFs for 50 times per temperature for the undamaged model. 500 diameters are randomly chosen within the 20 to 80 mm range for damaged signals at a specific temperature. PDFs of the properties are then sampled for each diameter, followed by FE model simulation. The permutation approach employed for the EXP dataset is replicated. The NUM dataset comprises all data derived from the numerical signals. In contrast, the HYB dataset amalgamates the EXP and NUM datasets. For diameters present in both the experimental and FE model datasets meant for training, only experimental data is incorporated into the HYB dataset. These datasets subsequently inform the training phase of a 1D CNN algorithm to assess damage size. Performance is gauged using validation and test subsets sourced from the EXP dataset. The distinguishing factor between these datasets is the origin of training data; the HYB dataset integrates both experimental readings and numerical data extracted from the Bayesian stochastic FE model. To avoid data unbalance in the HYB dataset, the number of experimental and numerical samples are mantained equal.

1D CNN structure definition The proposed 1D CNN consists of three sequence blocks of convolution-pooling-ReLU layers, followed by one fully connected layer, as presented in Tab. 8. The three blocks of 1D Convolutions + ReLU layers aim to extract features from the time series. The network has increasing filters along its dept, and the last layers comprise a sequence of flattened, fully connected, and regression layers. In this structure, the convolution part acts as a low-level feature extractor, while the fully connected part performs the regression based on such features. The last layer is a regression layer with a single neuron that predicts the diameter of the damage between 20 and 80 mm. The error is quantified using the mean squared error, the prediction, and the real value. The same structure is used in

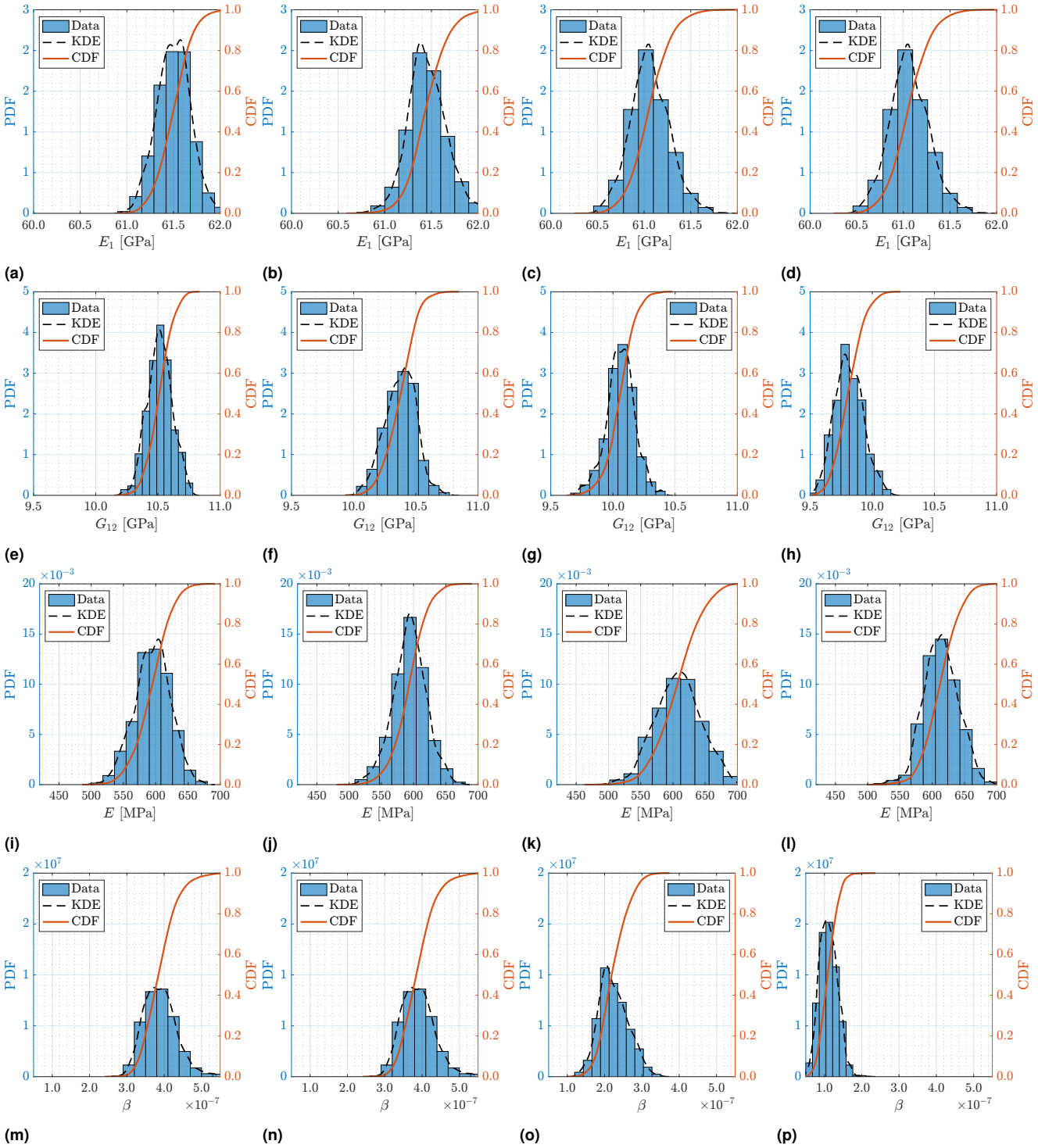

Figure 12. Results for stochastic updating procedure using 30, 50, and 70 mm damage diameters at 0, 10, 30, and 60°C, respectively, in the horizontal direction. (a) to (d) E_1 distribution; (e) to (h) G_{12} distribution; (i) to (l) E distribution; and (m) to (p) β bistribution. In the histograms, the colors represent: Sampled data (■), Kernel Density Estimate (KDE) (—) and Cumulative Density Function (CDF) (—).

	Temperature	**0 C**			**10 C**			**30 C**			**60 C**		
EXP	Undamaged signals	100			100			100			100		
	Damaged signals	700			700			700			700		
	Divide into	Train	Val.	Test	Train	Val.	Test	Train	Val.	Test	Train	Val.	Test
	Undamaged	30	15	55	15	30	55	30	15	55	15	30	55
	Damaged	200	100	400	100	200	400	200	100	400	100	200	400
	Possible combinations	6000	1500	22000	1500	6000	22000	6000	1500	22000	1500	6000	22000
FE	Undamaged signals	50			50			50			50		
	Damaged signals	500			500			500			500		
	Possible combinations	25000			25000			25000			25000		

Table 5. Experimental and FE model data division and number of samples.

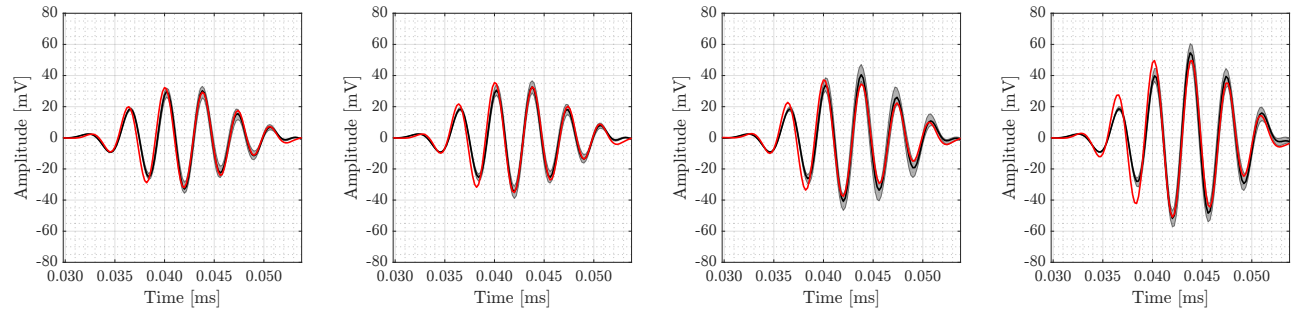

Figure 13. Model response for PZT at (a) 0 °C; (b) 10°C; (c) 30°C; and (d) 60°C. In the graphs, the colors represent experimental 50 mm damaged signal (—), model prediction for 50 mm with mean properties (—) and confidence interval (▬).

all training scenarios to evaluate the data impact on the 1D CNN's performance.

The internal structure of the network is evaluated through random search. For the first layer, two variables of interest are considered: kernel width and the number of filters per convolution. As the first layer is responsible for extracting basic features from the raw signal, the second and third kernel sizes are kept constant to reduce the hyperparameters search space. However, the number of filters is increased with the depth of the network; thus, the second and third layers have 2x and 3x times the number of filters of the first layer, respectively.

At the training stage, five hundred neural networks are simulated with hyperparameters sampled within the range: learning rate $\alpha \sim \mathcal{U}(0.1, 0.00001)$, kernel size $K \sim \mathcal{U}(3, 25)$, and the number of filters $N \sim \mathcal{U}(16, 32)$. It is worth noting that only odd numbers for the kernel size are evaluated to maintain symmetry around the convolution window. The adaptive moment estimation (Adam) training algorithm is used. The other training hyperparameters kept constant are presented in Tab. 6. Besides a maximum of 500 training epochs, early stop criteria are implemented to reduce overfitting. The validation data from the EXP dataset is used to evaluate (see Tab. 2) the loss and RMSE along the training are interrupted if validation loss increases in two subsequent epochs. The neural network structures are implemented on the MATLAB Deeplearning toolbox. All training rounds are carried out on a PC featuring AMD Ryzen 9 5950X CPU @ 3.40 GHz, 16 GB RAM, and an Nvidia GeForce 2060 GPU card using the GPU.

Training parameters	
Optimizer	Adam
β_1	0.9
β_2	0.999
ϵ	1E-8
L2 regularization factor	0.0001
Weight initializer	He
Total epochs	500
Mini-batch size	128

Table 6. Fixed training parameters.

The results and hyperparameters for the three best-performing networks are presented in Tab. 7 and are ordered based on the validation data error for the network trained with experimental data. The best networks exhibit similar errors in the training of the numerical network, rendering this criterion irrelevant to the selection process.

Figure 14 compares the networks of Tab. 7 during the experimental and hybrid data training stage. Networks 1 and 3 have learning rates in the same order of magnitude and the same kernel size, but network 1 has more filters. A larger number of filters results in a network with more parameters to train. Network 1 exhibits a higher tendency for instability in the validation data after a certain point, indicating overfitting to the training data. Network 2 encounters a similar stability issue and undergoes early stopping. Conversely, when examining the curve for case number 3, a more stable behavior throughout the training process is observed, allowing for additional training rounds.

Consequently, the network architecture is selected based on a trade-off between the error in experimental and hybrid training, the tendency to overfitting, and the training time required for the subsequent stages. Table 6 presents the parameters for the selected network.

Damage quantification The selected network is assessed using the EXP, NUM, and HYB datasets described in section Datasets preparation. The learning rate is initially set as 0.001 to minimize instability and subsequently fine-tuned throughout the process. An early stopping criterion based on the validation data error from the EXP dataset is employed. Training is stopped if the mean squared error decreases for two consecutive epochs. Figure 15 shows the training performance for each scenario.

The algorithm trained with the EXP dataset reaches a training error approximately 20% lower than the validation error, indicating overfitting to the training data. The algorithms trained with the NUM and HYB datasets exhibit comparable validation-to-training error ratios, although the HYB-trained algorithm demonstrates lower absolute error values. Furthermore, the algorithm trained with the HYB dataset achieves a lower validation error faster than the other two, which combined with the fact that the validation error is similar in the EXP and HYB strategies, demonstrates the

	Hyperparameters			Error at validation data		
Network	**Learning rate**	**Kernel size**	**Number of filters**	**EXP**	**NUM**	**HYB**
1	0.06720	19	31	0.0283	0.0817	0.0884
2	0.00360	3	24	0.0317	0.0819	0.0733
3	0.05640	19	20	0.0412	0.0780	0.0493

Table 7. Parameters and results on validation data for the 3 best networks at hyperparameters tuning phase.

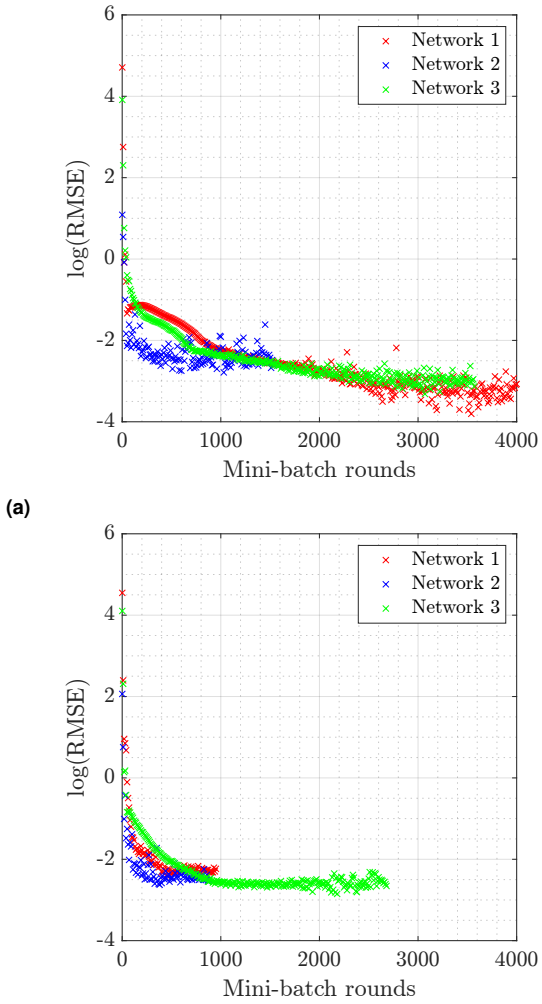

Figure 14. Validation RMSE for the three best networks with (a) EXP dataset; and (b) HYB dataset.

Layer	Type	Kernel	Stride
1	Input	-	-
2	1D convolution	19x20	1
3	Batch normalization	-	-
4	ReLU		-
5	Max pooling	-	2
6	1D convolution	10x40	1
7	Batch normalization	-	-
8	ReLU		-
9	Max pooling	-	2
10	1D convolution	10x60	1
11	Batch normalization	-	-
12	ReLU	5	-
13	Max pooling		2
14	Dropout	50%	-
15	Flatten		-
16	Fully connected		-

Table 8. Network structure used for regression.

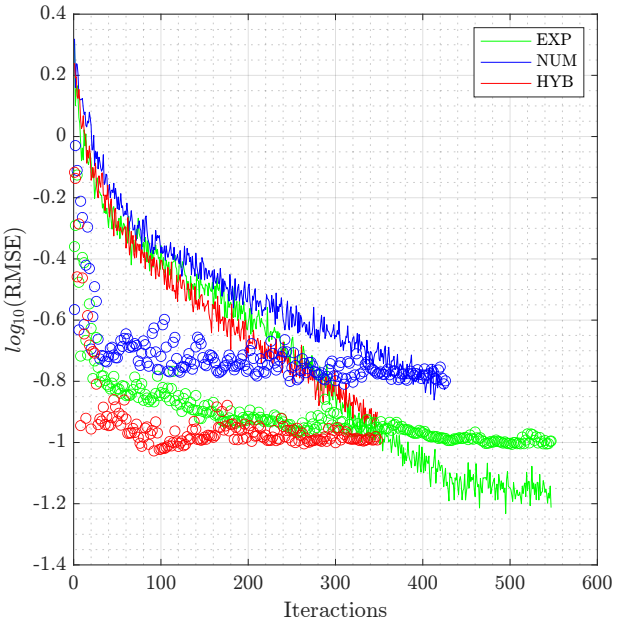

Figure 15. Comparison between training (—) and validation RMSE (○) for the EXP, NUM, and HYB training strategies.

greater robustness of the algorithm trained with the inclusion of data from the Bayesian stochastic FE model.

Table 9 summarizes the average results, with the model trained using the EXP dataset as the reference for error comparison. When evaluated on the test data, the model trained with the HYB dataset exhibits an average RMSE that is 87.5% of the model trained with the EXP dataset, resulting in a 12.5% reduction in error. The HYB model shows a 167% higher error on the training data than the EXP model. However, this difference can be attributed to the overfitting of the EXP model on the training data. Overfitting may lead to the model fitting too closely to the training data, resulting in poorer performance when faced with new, unseen data. Overfitting metrics reveal that the EXP model has validation/training and test/training ratios of 5.74 and 9.54, respectively, while the HYB model exhibits ratios of 2.16 and 3.11 for the same metrics. These findings suggest that the algorithm trained with the HYB dataset possesses superior generalization capabilities.

Conversely, training with the NUM dataset has a considerably higher error, as shown in Tab. 9. As this algorithm is trained with only numerical data and validated with experimental data for the early stopping criteria throughout the training, the training process stops when it starts to overfit the numerical data. Although the stochastic FE model replicates most of the signal within the confidence

interval, as seen in Figs. 13a to 13d, then the neural network starts to learn the particularities of the numerical signal and overfits after a certain training time. Additional tests on the NUM dataset have revealed that the proposed 1D CNN cannot effectively generalize when solely trained with numerical data in this experimental setup. Consequently, this model is not evaluated in the subsequent analysis.

Figure 16 compares the training strategies in terms of damage quantification on the experimental data. The confidence interval shown is derived from the 99% percentile of predictions on the training data. The neural network trained solely on experimental data exhibits a narrow confidence interval closely aligned with the optimal prediction region. However, this confidence interval does not accurately reflect reality due to its limited training data. All predictions for values in the test data lie outside the confidence interval, indicating the low reliability of this algorithm.

In contrast, the neural network trained with the HYB dataset demonstrates a more reliable confidence interval, as shown in Fig. 16a. Note that the confidence interval is narrow around the training diameters of 30, 50, and 70 mm and widens as it deviates from these regions. The network's training data includes experimental realizations at these diameters, leading to narrower confidence intervals. In contrast, the stochastic model generates the potential signals for other diameters in the analysis range. The neural network predictions trained with hybrid data mostly fall within the confidence interval, except for some predictions at 20 and 80 mm. These damages occur at the extreme ends of the FE model's validity range and in the extrapolation region of the experimental data used during training. Figure 16b shows that the neural network trained with the HYB dataset exhibits smaller errors within the interpolation range of the model. The error increases in regions near the validity limit of the stochastic model, but the network trained with the HYB dataset still shows less dispersion in its predictions.

Temperature influence Figure 17 displays predictions for damage size with training using the EXP and HYB datasets, divided by temperature. Upon evaluating the predictions, it is noticeable that the 1D CNN trained using the HYB dataset outperforms the one trained with the EXP dataset at all temperatures within the interpolation range (between 30 and 70 mm). Nevertheless, the algorithm trained with the HYB dataset exhibits lower error than the algorithm trained with the EXP dataset and can provide a similar confidence interval for multiple temperatures. Note that the model trained with the EXP dataset only has access to a single experimental condition for temperatures of 10°C and 60°C. Therefore, it lacks a confidence interval at these temperatures.

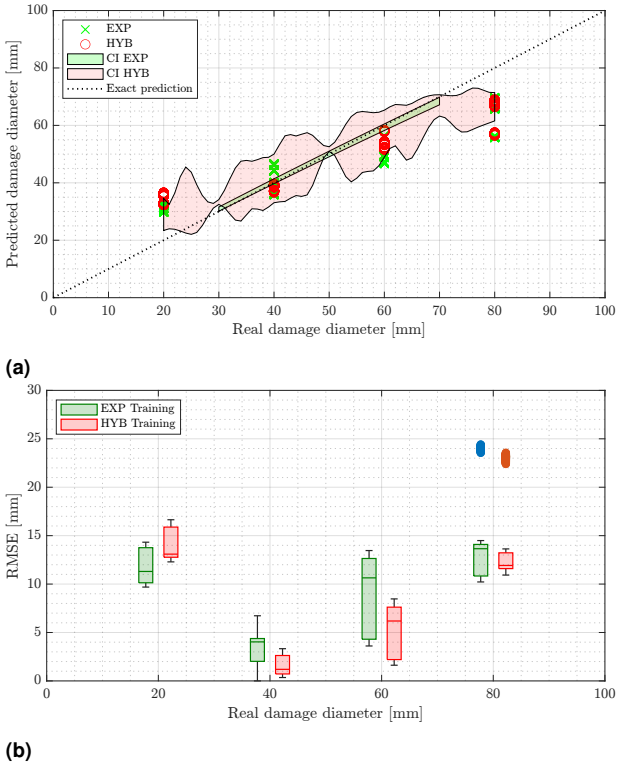

Figure 16. 1D CNN predictions for experimental test data: (a) Real and predicted damages along with confidence intervals (CI); and (b) RMSE concerning real diameter.

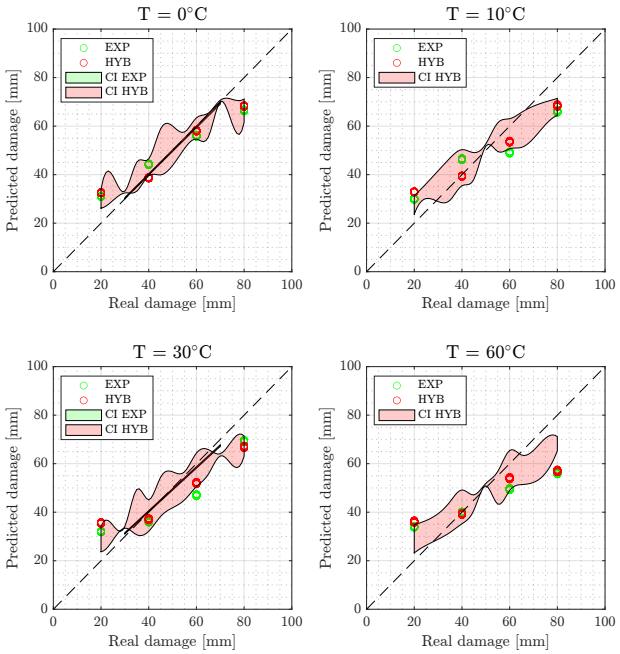

Figure 17. 1D CNN performance in different temperatures. CI represents the confidence intervals.

Discussions

As depicted in Figs 16 and 17, the machine learning algorithm trained with the proposed Bayesian data-driven strategy exhibits lower error and can provide reliable confidence intervals. Observing the narrower confidence interval at damage diameters where the experimental signal is used at the training step is possible. At the same time, it widens at diameters trained only with numerical data.

As the algorithm trained with the EXP and HYB datasets has to learn from both sources, it is harder to overfit the training data when compared to the model trained

Training strategy	EXP	NUM	HYB
Training RMSE (TR) [mm]	1.01	7.09	2.69
As EXP percentual	100%	705%	267%
Validation RMSE (VL) [mm]	5.77	9.46	5.83
As EXP percentual	100%	163%	101%
Test RMSE (TE) [mm]	9.59	12.3	8.38
As EXP percentual	100	128%	87.5%
Overfiting metrics			
VL/TR Ratio	5.74	1.33	2.16
TE/TR Ratio	9.54	1.73	3.11
TE/VL Ratio	1.66	1.30	1.44

Table 9. Summary of the quantification results.

with the EXP dataset. The latter presents a smaller error value on training data without a corresponding reduction in validation and test data. Despite resulting in a final validation error close to that observed in hybrid training, the ratio validation/training error is much higher for experimental training, indicating overfitting.

The region spanning from 30 to 70 mm corresponds to the interpolation segment of the training data, whereas 20 and 80 mm denotes extrapolation. Notably, the average error rises within the extrapolation regions. This can be attributed to both the inherent challenges associated with extrapolation and the proximity to the validity boundaries of the numerical model, which underwent validation between 20 and 80 mm.

Conversely, the network trained with the NUM dataset cannot achieve the same error level as the other two. It performs poorly in all scenarios due to the stopping criterion based on experimental data. Thus, it cannot train for sufficient time to adjust to the training data before the results diverge. For this network, the relaxation of the stopping criterion, allowing for more extended training, was evaluated. However, while the network improved performance on numerical data, it considerably worsened on experimental validation and testing data. Therefore, this training approach proved unfeasible with the given database, model, and training strategy.

Figure 17, note that the model exhibits superior performance at lower temperatures than higher ones. This phenomenon can be attributed to two factors. Firstly, the effect of the simulated damage on Lamb wave propagation is highly temperature-dependent due to the viscoelastic nature of the material used to simulate the damage, and its influence diminishes at higher temperatures. This reduction is mainly due to reduced damping, as shown in Figs. 13a to 13d. Secondly, the temperature range between the first three experimental datasets spans 30 degrees, while the difference between the 30 and 60-degree datasets is also 30 degrees. This requires the 1D CNN to work across a wider range at higher temperatures in addition to the reduced damage effect.

In situations with limited experimental data, algorithms trained solely on experimental data cannot provide a confidence interval, as was the case at 10°C and 60°C. Conversely, the CNN trained with the HYB dataset incorporates multiple potential signals generated by the stochastic model within its confidence interval, enabling the machine learning algorithm to establish its confidence intervals based on numerical data. The confidence intervals allow for greater confidence in the neural network's results, mitigate the black box nature typically associated with this algorithm, and allow one to explore the algorithm predictions across the proposed training scenarios.

Conclusions

The proposed Bayesian data-driven framework adeptly identifies and integrates vital FE model input parameters from experimental data while accounting for their inherent uncertainties. As a result, the stochastic FE model completes and enriches the existing dataset by providing simulated samples where data might be sparse. Combined with the potent generalization capabilities of CNNs, this approach yields a model that stands out in accelerated convergence, minimized validation and test errors, and superior resilience to temperature variations.

The samples proffered by the framework can be seamlessly merged during the training of machine learning algorithms, thereby enhancing their precision in damage quantification. As evidenced in the tests, the machine learning algorithm trained using this model-enhanced data achieved a 12.5% reduction in test data error compared to an algorithm trained using only experimental data. Moreover, this expanded dataset paves the way for establishing a confidence interval for model predictions. This addition significantly increases the reliability of results from the neural network, a crucial feature given the network's typical "black-box" nature.

In complicated scenarios characterized by diverse damage types and locations, the challenges faced by algorithms trained only on experimental data intensify. Our proposed framework demonstrates flexibility and efficiency in such situations, capable of handling a range of damage sizes and categories. The approach reduces the difficulty and amount of required experiments in a multidimensional landscape, offering an additional tool in situations where exhaustive factor combination testing is untenable. An example of a practical application could involve the analysis of delamination damage in various positions within

composite materials. Implementing the proposed framework on experimental data collected from specific positions within a delamination model integrated into a FE model enables the simulation of multiple additional damages through Bayesian updating. This approach trades machine time for substantial savings in time and costs typically linked with experimental setups.

CRediT authorship contribution statement

Leonardo Ferreira: Writing - original draft & editing, conceptualization, investigation, validation, software curation, writing - original draft & editing. **Rafael Teloli:** Writing - original draft reviewing& editing, conceptualization, formal analysis, supervision, . **Samuel da Silva:** Experimental setup design, experimental tests, writing - review, conceptualization, formal analysis, project administration. **Eloi Figueiredo:** Writing - original draft reviewing & editing, formal investigation. **Nuno Maia:** writing - review & editing, formal investigation, project administration. **Carlos Cimini:** Writing - review & editing, formal investigation, supervision.

Acknowledgments

The authors thank the financial support provided by Coordenação de Aperfeiçoamento de Pessoal de Nível Superior (CAPES/Brazil)-Finance Code 001 and CAPES/FCT grant number 2019.00164.CBM and The Portuguese National Funding Agency for Science Research and Technology (FCT/Portugal) for promoting the collaboration between Brazil/Portugal. Leonardo Ferreira acknowledges the funding from CAPES/Brazil grant number 88887.647575/2021-00. Samuel da Silva is thankful for the Brazilian National Council of Technological and Scientific Development (CNPq) grant number 306526/2019-0 and the São Paulo Research Foundation (FAPESP) grant number 19/19684-3. Eloi Figueiredo acknowledges the funding from FCT/Portugal through grant UIDB/ 04625/2020. Nuno Maia acknowledges the support of FCT/Portugal, through IDMEC, under LAETA, project UIDB/50022/2020. Carlos Cimini acknowledges the Fundação de Amparo à Pesquisa do Estado de Minas Gerais (Fapemig) through grant PPM-00422-18, and the CNPq through grant 304259/2021-7.

Declaration of Competing Interest

The authors declare that they have no known competing financial interests or personal relationships that could have appeared to influence the work reported in this paper.

Data availability

The raw data required to reproduce these findings can be downloaded from `https://github.com/shm-unesp/DATASET_PLATEUN01`.

References

1. Farrar CR, Doebling SW and Nix DA. Vibration-based structural damage identification. *Philosophical Transactions of the Royal Society A: Mathematical, Physical and Engineering Sciences* 2001; 359(1778): 131–149. DOI:10.1098/rsta.2000.0717.
2. Sarmadi H and Karamodin A. A novel anomaly detection method based on adaptive mahalanobis-squared distance and one-class knn rule for structural health monitoring under environmental effects. *Mechanical Systems and Signal Processing* 2020; 140: 106495. DOI:https://doi.org/10.1016/j.ymssp.2019.106495. URL `https://www.sciencedirect.com/science/article/pii/S0888327019307162`.
3. Mechbal N, Uribe JS and Rébillat M. A probabilistic multi-class classifier for structural health monitoring. *Mechanical Systems and Signal Processing* 2015; 60-61: 106–123. DOI:https://doi.org/10.1016/j.ymssp.2015.01.017. URL `https://www.sciencedirect.com/science/article/pii/S0888327015000230`.
4. Figueiredo E, Park G, Farrar CR et al. Three decades of statistical pattern recognition paradigm for shm of bridges. *Structural Health Monitoring* 2011; 10: 559–572. DOI:10.1177/1475921710388971. URL `https://doi.org/10.1177/1475921710388971`.
5. Lee IY, Jang J and Park YB. Advanced structural health monitoring in carbon fiber-reinforced plastic using real-time self-sensing data and convolutional neural network architectures. *Materials & Design* 2022; 224: 111348. DOI:https://doi.org/10.1016/j.matdes.2022.111348. URL `https://www.sciencedirect.com/science/article/pii/S0264127522009704`.
6. Wang D, He J, Guan X et al. A model assessment method for predicting structural fatigue life using Lamb waves. *Ultrasonics* 2018; 84: 319–328. DOI:10.1016/J.ULTRAS.2017.11.017.
7. Nagy PB, Simonetti F and Instanes G. Corrosion and erosion monitoring in plates and pipes using constant group velocity Lamb wave inspection. *Ultrasonics* 2014; 54(7): 1832–1841. DOI:https://doi.org/10.1016/j.ultras.2014.01.017. URL `https://www.sciencedirect.com/science/article/pii/S0041624X14000183`.
8. Tong T, Hua J, Lin J et al. Disbond contours evaluation in aluminum/CFRP adhesive joint based on excitation recovery of Lamb waves. *Composite Structures* 2022; 294: 115736. DOI:https://doi.org/10.1016/j.compstruct.2022.115736. URL `https://www.sciencedirect.com/science/article/pii/S0263822322005128`.
9. Boller C, Tomlinson GR and Staszewski WJ (eds.) *Health monitoring of aerospace structures : smart sensor technologies and signal processing*. Chichester, West Sussex, England ; Hoboken, NJ: J. Wiley, 2004. URL `https://onlinelibrary.wiley.com/doi/book/10.1002/0470092866`.

10. Zeng X, Liu X, Yan J et al. Lamb wave-based damage localization and quantification algorithms for CFRP composite structures. *Composite Structures* 2022; 295: 115849. DOI: 10.1016/J.COMPSTRUCT.2022.115849.
11. Konstantinidis G, Drinkwater BW and Wilcox PD. The temperature stability of guided wave structural health monitoring systems. *Smart Materials and Structures* 2006; 15(4): 967. DOI:10.1088/0964-1726/15/4/010. URL https://dx.doi.org/10.1088/0964-1726/15/4/010.
12. di Scalea FL and Salamone S. Temperature effects in ultrasonic lamb wave structural health monitoring systems. *The Journal of the Acoustical Society of America* 2008; 124: 161–174. DOI: 10.1121/1.2932071. URL https://doi.org/10.1121/1.2932071. Doi: 10.1121/1.2932071.
13. Mitra M and Gopalakrishnan S. Guided wave based structural health monitoring: A review. *Smart Materials and Structures* 2016; 25(5): 053001. DOI:10.1088/0964-1726/25/5/053001. URL https://dx.doi.org/10.1088/0964-1726/25/5/053001.
14. Zhang H, Hua J, Lin J et al. Damage localization with lamb waves using dense convolutional sparse coding network. *Structural Health Monitoring* 2022; 22: 1180–1192. DOI: 10.1177/14759217221092116.
15. Liu H and Zhang Y. Deep learning based crack damage detection technique for thin plate structures using guided lamb wave signals. *Smart Materials and Structures* 2019; 29: 15032. DOI:10.1088/1361-665X/ab58d6. URL https://dx.doi.org/10.1088/1361-665X/ab58d6.
16. Wu J, Xu X, Liu C et al. Lamb wave-based damage detection of composite structures using deep convolutional neural network and continuous wavelet transform. *Composite Structures* 2021; 276: 114590. DOI:10.1016/J.COMPSTRUCT.2021.114590.
17. Su C, Jiang M, Lv S et al. Improved damage localization and quantification of cfrp using lamb waves and convolution neural network. *IEEE Sensors Journal* 2019; 19(14): 5784–5791. DOI:10.1109/JSEN.2019.2908838.
18. Rai A and Mitra M. Lamb wave based damage detection in metallic plates using multi-headed 1-dimensional convolutional neural network. *Smart Materials and Structures* 2021; 30: 035010. DOI:10.1088/1361-665X/ABDD00.
19. Shao W, Sun H, Wang Y et al. A multi-level damage classification technique of aircraft plate structures using lamb wave-based deep transfer learning network. *Smart Materials and Structures* 2022; 31. DOI:10.1088/1361-665X/ac726f. URL https://doi.org/10.1088/1361-665X/ac726f.
20. Pandey P, Rai A and Mitra M. Explainable 1-d convolutional neural network for damage detection using lamb wave. *Mechanical Systems and Signal Processing* 2022; 164: 108220. DOI:10.1016/J.YMSSP.2021.108220.
21. Zhang S, Li CM and Ye W. Damage localization in plate-like structures using time-varying feature and one-dimensional convolutional neural network. *Mechanical Systems and Signal Processing* 2021; 147: 107107. DOI:https://doi.org/10.1016/j.ymssp.2020.107107. URL https://www.sciencedirect.com/science/article/pii/S0888327020304933.
22. Zhang H, Lin J, Hua J et al. Attention-based interpretable prototypical network towards small-sample damage identification using ultrasonic guided waves. *Mechanical Systems and Signal Processing* 2023; 188: 888–3270. DOI:10.1016/j.ymssp.2022.109990. URL https://doi.org/10.1016/j.ymssp.2022.109990.
23. Avci O, Abdeljaber O, Kiranyaz S et al. Structural damage detection in real time: Implementation of 1d convolutional neural networks for shm applications. Springer International Publishing. ISBN 978-3-319-54109-9, pp. 49–54.
24. Rai A and Mitra M. A transfer learning approach for damage diagnosis in composite laminated plate using lamb waves. *Smart Materials and Structures* 2022; 31(6): 065002. DOI:10.1088/1361-665X/ac66aa. URL https://dx.doi.org/10.1088/1361-665X/ac66aa.
25. Zhao C, Wen Y, Zhu J et al. Localization of surface dent deformation and inter-laminated damage in cfrp laminates under low-velocity impact behavior based on multi-channel one-dimensional convolutional gated recurrent unit. *Measurement* 2023; 221: 113503. DOI: https://doi.org/10.1016/j.measurement.2023.113503. URL https://www.sciencedirect.com/science/article/pii/S0263224123010679.
26. Kiranyaz S, Avci O, Abdeljaber O et al. 1d convolutional neural networks and applications: A survey. *Mechanical Systems and Signal Processing* 2021; 151: 107398. DOI:https://doi.org/10.1016/j.ymssp.2020.107398. URL https://www.sciencedirect.com/science/article/pii/S0888327020307846.
27. Xu Y, Kohtz S, Boakye J et al. Physics-informed machine learning for reliability and systems safety applications: State of the art and challenges. *Reliability Engineering and System Safety* 2023; 230. DOI:10.1016/J.RESS.2022.108900.
28. Zhang Z and Sun C. Structural damage identification via physics-guided machine learning: a methodology integrating pattern recognition with finite element model updating. *Structural Health Monitoring* 2020; 20: 1675–1688. DOI:10.1177/1475921720927488. URL https://doi.org/10.1177/1475921720927488. Doi: 10.1177/1475921720927488.
29. Wang L and Yuan FG. Group velocity and characteristic wave curves of Lamb waves in composites: Modeling and experiments. *Composites Science and Technology* 2007; 67: 1370–1384. DOI:10.1016/J.COMPSCITECH.2006.09.023.
30. Mead DJ. A general theory of harmonic wave propagation in linear periodic systems with multiple coupling. *Journal of Sound and Vibration* 1973; 27: 235–260.
31. Luca AD, Perfetto D, Fenza AD et al. Guided wave SHM system for damage detection in complex composite structure. *Theoretical and Applied Fracture Mechanics* 2020; 105. DOI: 10.1016/J.TAFMEC.2019.102408.
32. Ereiz S, Duvnjak I and Jiménez-Alonso JF. Review of finite element model updating methods for structural applications. *Structures* 2022; 41: 684–723. DOI:10.1016/J.ISTRUC.2022.05.041.
33. Lomazzi L, Fabiano S, Parziale M et al. On the explainability of convolutional neural networks processing ultrasonic guided waves for damage diagnosis. *Mechanical Systems and Signal Processing* 2023; 183: 109642. DOI:https://doi.org/10.1016/j.ymssp.2022.109642. URL https://www.sciencedirect.com/science/article/pii/S0888327022007282.
34. Mariani S, Rendu Q, Urbani M et al. Causal dilated convolutional neural networks for automatic inspection of ultrasonic signals in non-destructive evaluation and structural

health monitoring. *Mechanical Systems and Signal Processing* 2021; 157: 107748. DOI:https://doi.org/10.1016/j.ymssp.2021.107748. URL https://www.sciencedirect.com/science/article/pii/S0888327021001436.

35. Apalowo RK and Chronopoulos D. A wave-based numerical scheme for damage detection and identification in two-dimensional composite structures. *Composite Structures* 2019; 214: 164–182. DOI:10.1016/J.COMPSTRUCT.2019.01.098.
36. Paćko P, Bielak T, Spencer AB et al. Lamb wave propagation modelling and simulation using parallel processing architecture and graphical cards. *Smart Materials and Structures* 2012; 21(7): 075001. DOI:10.1088/0964-1726/21/7/075001. URL https://dx.doi.org/10.1088/0964-1726/21/7/075001.
37. Wang X, Hill TL, Neild SA et al. Model updating strategy for structures with localised nonlinearities using frequency response measurements. *Mechanical Systems and Signal Processing* 2018; 100: 940–961. DOI:10.1016/J.YMSSP.2017.08.004.
38. de O Teloli R, da Silva S, Ritto TG et al. Bayesian model identification of higher-order frequency response functions for structures assembled by bolted joints. *Mechanical Systems and Signal Processing* 2021; 151. DOI:10.1016/J.YMSSP.2020.107333.
39. Miguel LP, Teloli RO and da Silva S. Bayesian model identification through Harmonic Balance Method for hysteresis prediction in bolted joints. *Nonlinear Dynamics* 2022; 107(1): 77–98. DOI:https://doi.org/10.1007/s11071-021-06967-2.
40. Ritto TG, Sampaio R and Aguiar RR. Uncertain boundary condition bayesian identification from experimental data: A case study on a cantilever beam. *Mechanical Systems and Signal Processing* 2016; 68-69: 176–188. DOI:10.1016/J.YMSSP.2015.08.010.
41. Jaboviste K, Sadoulet-Reboul E, Teloli RO et al. Characterizing the nonlinear behavior of viscoelastic materials: A Bayesian approach combining Oberst beam experiments and digital-twin simulations. *Mechanical Systems and Signal Processing* 2024; 208: 110978. DOI:https://doi.org/10.1016/j.ymssp.2023.110978. URL https://www.sciencedirect.com/science/article/pii/S0888327023008865.
42. Gallina A, Ambrozinski L, Packo P et al. Bayesian parameter identification of orthotropic composite materials using lamb waves dispersion curves measurement. *Journal of Vibration and Control* 2017; 23: 2656–2671. DOI:10.1177/1077546315619264. URL https://doi.org/10.1177/1077546315619264.
43. Yan WJ, Chronopoulos D, Cantero-Chinchilla S et al. A fast Bayesian inference scheme for identification of local structural properties of layered composites based on wave and finite element-assisted metamodeling strategy and ultrasound measurements. *Mechanical Systems and Signal Processing* 2020; 143. DOI:10.1016/J.YMSSP.2020.106802.
44. de Paula S Ferreira L, de O Teloli R, da Silva S et al. Bayesian calibration for lamb wave propagation on a composite plate using a machine learning surrogate model. *Mechanical Systems and Signal Processing* 2024; 208: 111011. DOI:https://doi.org/10.1016/j.ymssp.2023.111011. URL https://www.sciencedirect.com/science/article/pii/S0888327023009196.
45. Paixão J, da Silva S, Figueiredo E et al. Delamination area quantification in composite structures using gaussian process regression and auto-regressive models. *Journal of Vibration and Control* 2021; 27(23-24): 2778–2792. DOI:10.1177/1077546320966183. URL https://doi.org/10.1177/1077546320966183. https://doi.org/10.1177/1077546320966183.
46. da Silva S, Paixão J, Rébillat M et al. Extrapolation of ar models using cubic splines for damage progression evaluation in composite structures. *Journal of Intelligent Material Systems and Structures* 2020; 32: 284–295. DOI:10.1177/1045389X20963171. URL https://doi.org/10.1177/1045389X20963171. Doi: 10.1177/1045389X20963171.
47. da Silva S and Paixão J. Unesp-concept: Carbon-epoxy composite plate, 2020. DOI:10.13140/RG.2.2.35767.34722.
48. Bud MA, Moldovan I, Radu L et al. Reliability of probabilistic numerical data for training machine learning algorithms to detect damage in bridges. *Structural Control and Health Monitoring* 2022; 29(7): e2950. DOI:https://doi.org/10.1002/stc.2950. URL https://onlinelibrary.wiley.com/doi/abs/10.1002/stc.2950.
49. da S Raqueti R, de O Teloli R, da Silva S et al. On the use of stochastic Bouc–Wen model for simulating viscoelastic internal variables from a finite element approximation of steady-rolling tire. *Journal of Vibration and Control* 0; 0(0): 10775463221125038. DOI:10.1177/10775463221125038. URL https://doi.org/10.1177/10775463221125038.
50. Saltelli A, Ratto M, Andres T et al. *Global sensitivity analysis: the primer*. John Wiley & Sons, 2008.
51. Marelli S and Sudret B. UQLab: A framework for uncertainty quantification in Matlab. In *Vulnerability, Uncertainty, and Risk*. ASCE Reston, VA, 2014. pp. 2554–2563. DOI:10.1061/9780784413609.257. URL https://ascelibrary.org/doi/abs/10.1061/9780784413609.257.
52. Lye A, Cicirello A and Patelli E. Sampling methods for solving Bayesian model updating problems: A tutorial. *Mechanical Systems and Signal Processing* 2021; 159: 107760. DOI:https://doi.org/10.1016/j.ymssp.2021.107760. URL https://www.sciencedirect.com/science/article/pii/S0888327021001552.
53. Hornik K, Stinchcombe M and White H. Multilayer feedforward networks are universal approximators. *Neural Netw* 1989; 2(5): 359–366.
54. Fakih MA, Chiachío M, Chiachío J et al. A Bayesian approach for damage assessment in welded structures using Lamb-wave surrogate models and minimal sensing. *NDT and E International* 2022; 128. DOI:10.1016/J.NDTEINT.2022.102626.
55. Kiranyaz S, Avci O, Abdeljaber O et al. 1d convolutional neural networks and applications: A survey. *Mechanical Systems and Signal Processing* 2021; 151: 107398. DOI:https://doi.org/10.1016/j.ymssp.2020.107398. URL https://www.sciencedirect.com/science/article/pii/S0888327020307846.
56. Lee JS, Park G, Kim CG et al. Use of relative baseline features of guided waves for in situ structural health monitoring. *Journal of Intelligent Material Systems and Structures* 2011; 22: 175–189. DOI:10.1177/1045389X10395643. URL https://doi.org/10.1177/1045389X10395643.

Doi: 10.1177/1045389X10395643.

57. Gresil M, Giurgiutiu V, Shen Y et al. Guidelines for using the finite element method for modeling of guided Lamb wave propagation in shm processes. *e-Journal of Nondestructive Testing (eJNDT) 1435-4934* 2013; URL https://www.ndt.net/search/docs.php3?id=14011.
58. Sirohi J and Chopra I. Fundamental understanding of piezoelectric strain sensors. *Journal of Intelligent Material Systems and Structures* 2000; 11(4): 246–257. DOI:10.1106/8BFB-GC8P-XQ47-YCQ0. URL https://doi.org/10.1106/8BFB-GC8P-XQ47-YCQ0.
59. Moser F, Jacobs LJ and Qu J. Modeling elastic wave propagation in waveguides with the finite element method. *NDT and E International* 1999; 32: 225–234. DOI:10.1016/S0963-8695(98)00045-0.
60. Wan HP, Mao Z, Todd MD et al. Analytical uncertainty quantification for modal frequencies with structural parameter uncertainty using a gaussian process metamodel. *Engineering Structures* 2014; 75: 577–589. DOI: https://doi.org/10.1016/j.engstruct.2014.06.028. URL https://www.sciencedirect.com/science/article/pii/S0141029614003848.
61. Wan HP and Ren WX. Stochastic model updating utilizing bayesian approach and gaussian process model. *Mechanical Systems and Signal Processing* 2016; 70-71: 245–268. DOI:https://doi.org/10.1016/j.ymssp.2015.08.011. URL https://www.sciencedirect.com/science/article/pii/S0888327015003726.
62. Liu Z, Lesselier D, Sudret B et al. Surrogate modeling based on resampled polynomial chaos expansions. *Reliability Engineering & System Safety* 2020; 202: 107008. DOI:https://doi.org/10.1016/j.ress.2020.107008. URL https://www.sciencedirect.com/science/article/pii/S0951832020305093.
63. Lim H and Manuel L. Distribution-free polynomial chaos expansion surrogate models for efficient structural reliability analysis. *Reliability Engineering & System Safety* 2021; 205: 107256. DOI:https://doi.org/10.1016/j.ress.2020.107256. URL https://www.sciencedirect.com/science/article/pii/S0951832020307560.
64. Zhou L, Wang L, Chen L et al. Structural finite element model updating by using response surfaces and radial basis functions. *Advances in Structural Engineering* 2016; 19: 1446–1462. DOI:10.1177/1369433216643876. URL https://doi.org/10.1177/1369433216643876.
65. Padil KH, Bakhary N and Hao H. The use of a non-probabilistic artificial neural network to consider uncertainties in vibration-based-damage detection. *Mechanical Systems and Signal Processing* 2017; 83: 194–209. DOI:https://doi.org/10.1016/j.ymssp.2016.06.007. URL https://www.sciencedirect.com/science/article/pii/S0888327016301893.